Case Studies in Construction Materials 22 (2025) e04209

Contents lists available at ScienceDirect

Case Studies in Construction Materials

journal homepage: www.elsevier.com/locate/cscm

# Predictive modeling for durability characteristics of blended cement concrete utilizing machine learning algorithms

Bo Fu [a,*], Hua Lei [a], Irfan Ullah [b], Mohammed El-Meligy [c,d], Khalil El Hindi [e], Muhammad Faisal Javed [f,g], Furqan Ahmad [h,*]

[a] Collage of Civil Engineering, North Minzu University, Yinchuan 750021, China
[b] Department of Civil and Transportation Engineering, Hohai University, Nanjing, China
[c] Applied Science Research Center, Applied Science Private University, Amman, Jordan
[d] Jadara University Research Center, Jadara University, PO Box 733, Irbid, Jordan
[e] Department of Computer Science, College of Computer & Information Sciences, King Saud University, Riyadh 11543, Saudi Arabia
[f] Department of Civil Engineering, GIK Institute of Engineering Sciences and Technology, Swabi 23640, Pakistan
[g] Western Caspian University, Baku, Azerbaijan
[h] UNHCR, Afghanistan

ARTICLE INFO

*Keywords:*
Blended cement concrete
Machine learning
Gene expression programming
Multiple expression programming

ABSTRACT

Chloride penetration and carbonation resistance are critical durability attributes that assess concrete's ability to withstand challenging environmental conditions. However, determining these parameters requires time-consuming and resource-intensive physical experiments. Accordingly, this study employed gene expression programming (GEP) and multi-expression programming (MEP) to develop a robust model for predicting these parameters, providing mathematical equations for their estimation. Additionally, the study to develop a graphical user interface that would allow for predictions based solely on input values, thereby eliminating the need for extensive physical testing. To thoroughly assess the effectiveness of the proposed GEP and MEP models, a range of statistical metrics were employed, including the coefficient of determination ($R^2$), adjusted $R^2$, root mean square error (RMSE), mean absolute error (MAE), and root mean square error to observation's standard deviation ratio (RSR), along with engineering indices like the a10-index and a20-index. Both GEP and MEP models consistently demonstrated outstanding performance across all statistical indicators for both carbonation rate and chloride

*Abbreviations:* OPC, Ordinary Portland Cement; $CO_2$, Carbon dioxide; BCC, Blended cement concrete; SCMs, Supplementary cementitious materials; BFS, Blast furnace slag; FA, Fly ash; SF, Silica fume; CEM III/A, Type III/A cement; CEM III/B, Type III/B cement; CEM II/B-V, Type II/B-V cement; VA, Volcanic ash; VP, Volcanic pumice; CCA, Corn Cob Ash; GGBS, Ground granulated blast furnace slag; C3A, Tricalcium aluminate; RC, Reinforced concrete; PH, Potential of Hydrogen; RH, Relative humidity; CaO, Calcium oxide; PC, Polycarboxylic acid; NS, Naphthalene sulfonate; ML, Machine learning; DT, Decision tree; R, Correlation coefficient; AR, AdaBoost regressor; BO-XGBoost, Bayesian optimization extreme gradient boosting; $R^2$, Coefficient of determination; KNN, K-nearest neighbor; RF, Random forest; ANN, Artificial neural network; SVM, Support vector machine; CSA, Coupled simulated annealing; LSSVM, Least squares support vector machine; GEP, Gene expression programming; MEP, Multi-expression programming; ANFIS, Adaptive neuro-fuzzy inference system; GB, Gradient boost; XGB, Extreme gradient boosting; OGPR, Optimized gaussian process regression; AB, AdaBoost; BR, Bagging regressor; MAPE, Mean absolute percentage error; RMSE, Root mean square error; WTRP, Waste tire rubber powder; SHAP, SHapely Additive exPlanations; PDP, Partial dependence plot.

* Corresponding authors.
*E-mail addresses:* 2015006@nmu.edu.cn (B. Fu), 18195140189@163.com (H. Lei), 19pwciv5205@uetpeshawar.edu.pk (I. Ullah), mohammedali2000@gmail.com (M. El-Meligy), khindi@ksu.edu.sa (K. El Hindi), arbabfaisal@giki.edu.pk (M.F. Javed), engr.furqanahmad123@gmail.com (F. Ahmad).

https://doi.org/10.1016/j.cscm.2025.e04209
Received 3 July 2024; Received in revised form 11 November 2024; Accepted 1 January 2025
Available online 3 January 2025

penetration. The GEP model showed high precision in modeling chloride penetration with an $R^2$ of 0.954, MAE of 0.252, and RMSE of 1.050, and for carbonation rate with an $R^2$ of 0.99, MAE of 0.230, and RMSE of 1.100. Similarly, the MEP model performed well, achieving an $R^2$ of 0.913, MAE of 0.489, and RMSE of 1.434 for chloride penetration, and an $R^2$ of 0.985, MAE of 0.560, and RMSE of 1.440 for carbonation rate. In addition, the SHapley Additive exPlanation (SHAP) method was employed to comprehend the model estimations. In predicting chloride penetration, cement to water ratio (C/B) emerged as the most impactful feature, followed by silica fume to binder ratio (SF/B) and water to binder ratio (W/B) in terms of importance. For carbonation rate, W/B stood out as the most influential, with C/B and fly ash to binder ratio (FA/B) being the subsequent key factors. These intuitions are further supported by partial dependence plots (PDPs). Furthermore, the SHAP summary plots distinctly reveal the relationships between the various parameters and the estimated characteristics.

## 1. Introduction

Ordinary Portland Cement (OPC), comprising 10–12 % of concrete, is energy-intensive, emitting 0.85 tons of $CO_2$ per ton produced, with global output now over 3 billion tons annually [1]. To lessen concrete's environmental impact, researchers are exploring alternative materials to partially replace OPC. Blended cement concrete (BCC) is a concrete variety that includes a mixture of different cementitious materials alongside or in place of traditional Portland cement [2]. These supplementary cementitious materials (SCMs), like blast furnace slag (BFS), fly ash (FA), silica fume (SF), and natural pozzolans, can improve the properties of concrete, including durability, workability, and environmental sustainability [3]. The lifespan of blended cements having greater levels of cement substitution, such as CEM III/A (containing 50 % BFS), CEM III/B (with 80 % BFS), and CEM II/B-V (incorporating 35 % FA), was approximately reduced by 10 % owing to an increased coefficient of carbonation rate. Despite the decreased capture of carbon dioxide and lifespan compared to Portland cement, CEM III/B produced 20 % fewer $CO_2$ annually [4]. Volcanic ash (VA), BFS, FA, volcanic pumice (VP), SF, and similar materials are utilized as substitutes for cement. These materials generally enhance the durability of concrete and decrease the heat generated during hydration, which is advantageous for applications involving mass concrete [5]. The slump of corn cob ash (CCA) concrete and compacting factor showed reduction with increasing CCA content, indicating reduced workability and increased stiffness. Initially, the crushing strength of CCA-blended cement concrete was lower than that of the control mix during beginning phases, but it notably improved and exceeded the control's strength in later phases, specifically after 120 days [6]. It was noted that the alkalinity and strength of the BCC was comparable to those of ordinary concrete. Moreover, the pH levels of the BCC exceeded the recommended limit for depassivation [7]. The effectiveness of various pozzolans in enhancing strength becomes

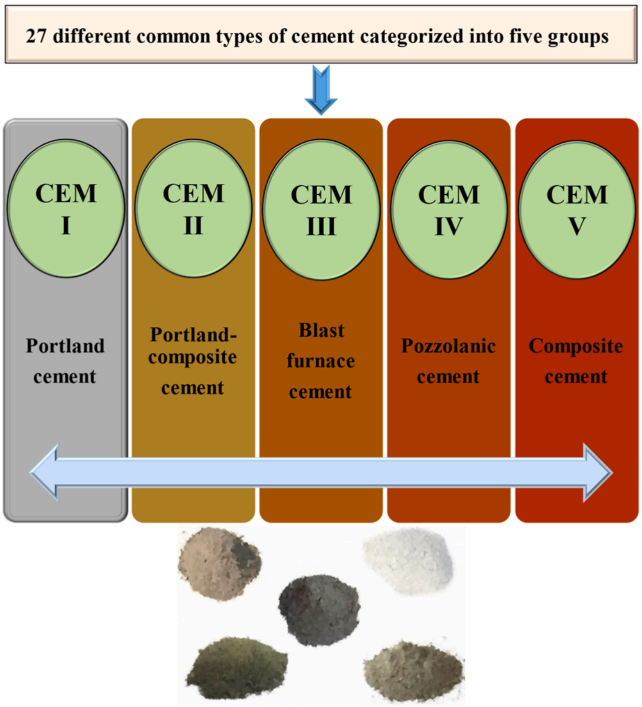


**Fig. 1.** Types of cement (EN 107–1).

more evident when used as additives in blended cement concrete. The 28-day strength improvement in concrete, in contrast to the control mix, reached up to 75 % for silica fume, 45 % for metakaolin, 27 % for fly ash, and 40 % for ground granulated slag (GGBS). Similarly, when these pozzolans replaced part of the cement, the strength enhancements were up to11 % for GGBS, 50 % for silica fume, 3 % for metakaolin, and 9 % for fly ash [8]. BCC mixtures incorporating type I/V (low $C_3A$) cement with VA or finely ground VP demonstrated reduced durability performance in comparison to type I/V plain cements over a 48-month period [9]. Alkali concentrations typically decrease as the replacement of PC with SCMs increases. This decrease in alkali levels within the pore solution results in lower hydroxide ion concentrations. Sulfate concentrations are not significantly impacted by blending with GGBS or FA [10]. The European standard EN 197–1 categorizes cement into 27 distinct common types, organized into five groups, as depicted in Fig. 1.

Chloride penetration and carbonation resistance are critical durability attributes that evaluate concrete's ability to withstand challenging environmental conditions. These characteristics play a vital role in the longevity, durability, and overall functionality of concrete structures, highlighting their importance in assessing extended-term robustness [3]. Corrosion in reinforced concrete (RC) is primarily induced by chloride infiltration. Chloride-induced corrosion initiates upon reaching a critical concentration of chloride ions at the steel bars, causing the breakdown of a thin protective layer of corrosion products. The presence of this protective layer, which develops as a result of the elevated alkaline environment of concrete during construction completion, protects the steel bars against corrosion [11]. Carbonation occurs when $CO_2$ penetrates the porous system of concrete, creating a lower pH environment around the reinforcement, which allows corrosion to occur [12]. The depth of carbonation is commonly utilized to forecast the lifespan of concrete. The pivotal factors that significantly influence carbonation resistance of concrete include relative water-cement ratio and humidity (RH) [13]. The resistance of mortar and concrete to carbonation mainly depends on the $CO_2$ buffering capacity per unit volume of cement paste. This can be quantified as the proportion of water used during production to the quantity of reactive CaO in the binder [14]. The polycarboxylic acid (PC) superplasticizer significantly enhances concrete's carbonation resistance, though increasing its dosage does not amplify this effect. Naphthalene sulfonate (NS) superplasticizer also improves anti-carbonation. Both superplasticizers influence carbonation resistance by altering the pore structures and morphologies of the concrete, thereby reducing its porosity [15]. The effect of substituting OPC with SCMs on the resulting concrete varies significantly based on the variety of SCM, its quantity, and the blend design. Therefore, enhancing the attributes of BCC with one or more SCMs to create a green concrete blend is challenging, laborious, and feasible solely through individualized experimental analysis for each case. This highlights the necessity to estimate the characteristics of a BCC mix and minimize the scope of the experimental study [2].

Machine learning (ML) methods provide an effective solution by efficiently capturing these complex relationships, significantly reducing the computational costs associated with physically-based models [16]. The decision tree (DT) model effectively predicted the compressive strength of BCC mixes, achieving a high correlation coefficient (R) of 0.99 in both the training and validation datasets. The AdaBoost regressor (AR) model predicted both durability characteristics of BCC with an R-value over 0.98 [3]. Machine learning approaches were applied to high-strength ternary blended concrete with varying silica quantities. Both BO-XGBoost and linear regression demonstrated higher coefficients of determination ($R^2$) and lower error values compared to the KNN model, indicating better predictive success. For instance, the $R^2$ values were 0.883 for linear regression, 0.736 for k-nearest neighbor (KNN), and 0.880 for BO-XGBoost [17]. Numerous models, encompassing random forest (RF), artificial neural network (ANN), SVM, and DT, have been developed to predict ternary-blend concrete compressive strength. Coupled simulated annealing (CSA) was utilized to fine-tuned the least square support vector machine (LSSVM) model. The LSSVM model outperformed others, achieving an $R^2$ value of 0.954 [18]. Three ML approaches, namely genetic programming, water cycle algorithm, and soccer league competition programming, were developed for designing sustainable concrete mixtures. Their accuracy was compared to three conventional methods: support vector machine, artificial neural network, and linear regression [19]. An exhaustive dataset of concrete and corresponding disruptive laboratory assessments was utilized to train the selected best configuration of an ANN. The final ANN model adopted has four predictors, six hidden neurons, four principal components, and one response parameter [20]. A RF model was used to attain high-fidelity forecasts of time-sensitive hydration kinetics in systems based on OPC. The results indicate that the RF model is capable of developing mixture designs that align with user-defined kinetics-related requirements [21]. The multilayer perceptron model showed high effectiveness for predicting the growth of static yield stress in blended cement pastes [22]. Various models, encompassing gene expression programming (GEP), ANN, support vector (SV), RF, adaptive neuro-fuzzy inference system (ANFIS), gradient boost (GB), extreme gradient boost (XGB), optimized gaussian process regression (OGPR), KNN, adaBoost (AB), and bagging regressor (BR), were used to estimate compressive strength. The XGB model attained the greater efficacy, with an $R^2$ score of 0.89 [23]. Random forest, AdaBoost, SVM, and Bayes classifier ML models were employed to estimate properties of blast furnace slag (BFS) and waste tire rubber powder (WTRP) blended cement mortar. Among these algorithms, AB showed the best performance with $R^2$, mean absolute percentage error (MAPE), root mean square error (RMSE), and scores of 5.2425, 0.9831, and 0.1105, respectively [24].

Blended cement substantially influences the characteristics of concrete, particularly impacting its chloride ion penetrability and carbonation rate. These are critical durability attributes that assess concrete's ability to withstand challenging environmental conditions. However, determining these parameters requires time-consuming and resource-consuming physical experiments. Accordingly, this study employed gene expression programming (GEP) and multi-expression programming (MEP) to develop a robust model for predicting these parameters. MEP and GEP offer clear interpretability by providing explicit mathematical expressions that reveal the relationships between inputs and outputs, making them more transparent. Both methods naturally perform feature selection, adapt to various problem types, and are computationally efficient, requiring minimal training and resources compared to deep learning. They excel with small datasets and can produce empirical equations ideal for practical applications in engineering, where simplicity, transparency, and robustness are essential for reliable predictions. Additionally, the study to develop a graphical user interface that would allow for predictions based solely on input values, thereby eliminating the need for extensive physical testing.

## 2. Overview of ML approaches employed

This section entails the theory of ML techniques utilized.

### 2.1. Gene expression programming

GEP was introduced by Ferreira in 1999 as an innovative algorithm that integrates aspects of Genetic Algorithms (GA) and Genetic Programming (GP). GEP marks a major advancement by exceeding the phenotype threshold, the second evolutionary threshold, through the isolation of phenotype and genotype [25]. GEP is a well-known Evolutionary Algorithm (EA) designed to solve user-defined problems by evolving computer programs. In GEP, these programs are typically represented by gene expression strings of fixed length, which undergo natural operations like crossover and mutation. GEP has demonstrated to be an efficient approach for creating clear and precise programs [26]. Lately, GEP has seen significant advancements and developments. Numerous improved versions of GEP have been suggested, and their practical applications are rapidly increasing [26]. GEP is an innovative EA that addresses many of the limitations found in traditional GA and GP. In GEP, the chromosome is responsible for encoding the potential solution, which is then interpreted as an expression tree, symbolizing the real solution. This conventional method is analogous to the translation of genetic information from DNA into proteins in biological systems. The genetic operators of GEP are employed to the chromosome itself, rather than directly to the expression tree [27]. Fig. 2 illustrates the process flow of GEP, while Fig. 3 depicts the chromosome expression tree.

### 2.2. Multi expression programming

MEP is a variant of GP that employs a linear format for chromosomes. MEP individuals consist of gene sequences that encode intricate computer programs. The format of MEP individuals, representing expressions, bears similarity to how compilers convert C or Pascal expressions into machine code [28]. MEP possesses a distinctive capability to encode numerous programs related to a problem in a single chromosome. Numerical tests have demonstrated MEP's superiority over comparable methods, positioning it as an effective substitute for conventional tree-based Genetic Programming [29]. MEP stands out from other methods by improving efficiency and reducing computation time through its linear-based approach and the inclusion of multiple solutions within each chromosome. The results from MEP are represented as linear instruction strings, combining mathematical operators (functions) and variables (terminals). The chromosome's length is determined by the quantity of MEP genes per chromosome, offering a flexible and adaptable framework for problem-solving [30]. An MEP chromosome comprises several expressions, corresponding to the number of genes it holds. This multi-expression structure transforms an MEP chromosome into a collection of trees rather than a singular tree. Each of these expressions represents a potential solution to a given problem. The overall fitness of an MEP chromosome is gauged by the fitness level of the best expression it encodes [31]. The process flow of MEP is illustrated in Fig. 4.

## 3. Methodology

### 3.1. Description of database

The database employed comprised 362 sets of experimental data for carbonation rate and 326 sets for chloride penetration, collected from various literature sources [4,14,32–157]. The predictor variables used in this study include binder (B), cement to binder

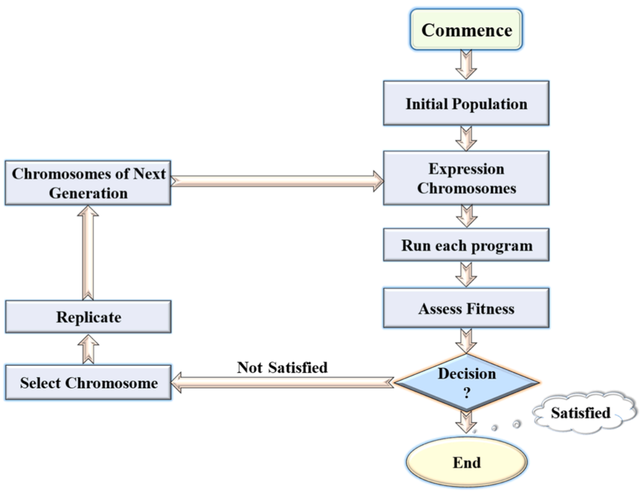


**Fig. 2.** Process flow of GEP.

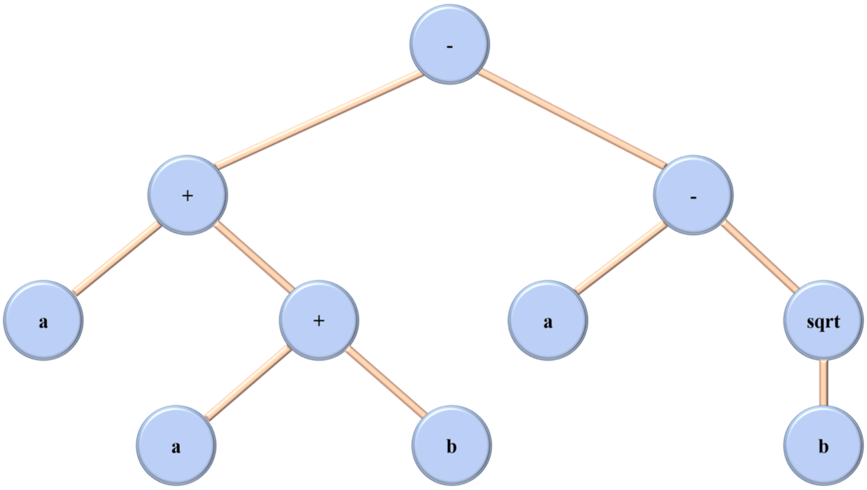


**Fig. 3.** Chromosome expression tree.

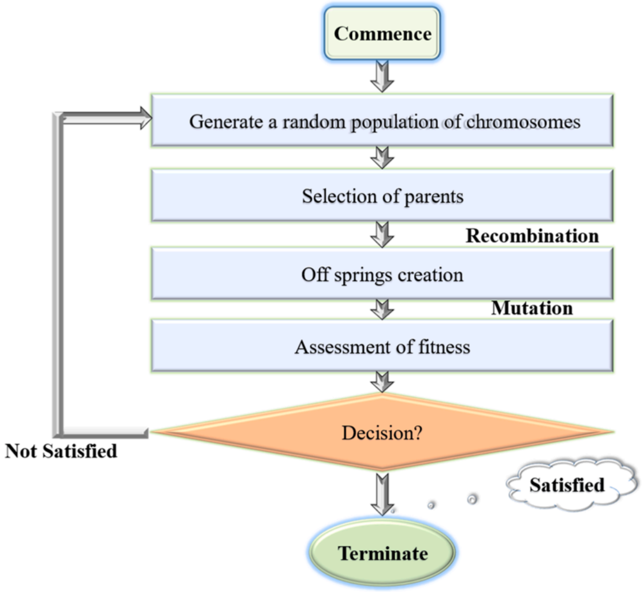


**Fig. 4.** Process flow of MEP.

ratio (C/B), water to binder ratio (W/B), ground granulated blast furnace slag to binder ratio (GGBF/B), fly ash to binder ratio (FA/B), silica fume to binder ratio (SF/B), limestone powder to binder ratio (LP/B), calcined clay to binder ratio (CCl/B), fine aggregate to binder ratio (FiA/B), coarse aggregate to binder ratio (CoA/B), and superplasticizer to binder ratio (SP/B). The target variables (TV) are chloride penetration and carbonation rate of BCC. Fig. 5 illustrates the predictors and response parameters. For the training of the chloride penetration model, 70 % of the database comprising 228 data points is allocated, while the remaining 30 %, totaling 98 data points, is dedicated to testing. Likewise, in the training phase of the carbonation rate model, 70 % of the dataset consisting of 253 data points is utilized, with the remaining 30 %, amounting to 109 data points, reserved for testing purposes. This random partitioning ensures that the model has an adequate amount of data to learn and recognize patterns, thereby enhancing its generalization ability. The larger training set enables the model to capture intricate relationships within the data, while the test set serves as a reliable measure of the model's performance and its ability to make accurate predictions on unseen data [158–160]. Table 1 presents statistical data on carbonation rate and chloride penetration in concrete, detailing various parameters like mean, median, mode, standard deviation, maximum, minimum, and skewness. For carbonation rate, the mean is 363.02 mm/year$^{0.5}$, with a median of 350.00 mm/year$^{0.5}$ and a mode of 400.00 mm/year$^{0.5}$. The maximum and minimum values are 635.00 mm/year$^{0.5}$ and 204.00 mm/year$^{0.5}$, respectively. Chloride penetration shows a mean of 405.37 Coulombs, with a median of 400.00 Coulombs and a mode of 400.00 Coulombs. The maximum chloride penetration is 600.00 Coulombs, while the minimum is 237.00 Coulombs. Both

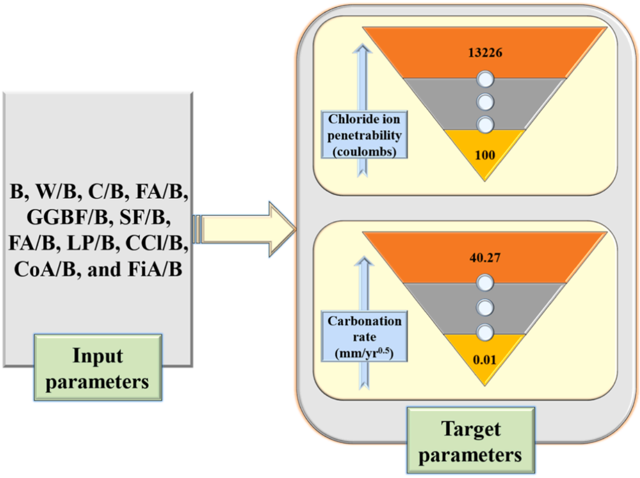


**Fig. 5.** Predictors and response parameters.

parameters exhibit notable skewness, indicating the distribution asymmetry in the data. Chloride penetrability based on charge passed is illustrated in Fig. 6. Box plots of the response parameters are presented in Fig. 7.

Fig. 8 depicts the correlation heatmaps. The Pearson correlation matrix shows that chloride penetration correlates positively with C/B (0.39), Co/B (0.27), and W/B (0.24),and negatively with SF/B (-0.34), FA/B (-0.23), and GGBF/B (-0.17)Similarly, the Spearman correlation matrix shows positive correlations with C/B (0.45), W/B (0.26), and CoA/B (0.20), and negative correlations with SF/B (-0.39), FA/B (-0.23), and Cl/B (-0.19).For carbonation rate, the Pearson matrix indicates positive correlations with CoA/B (0.27), W/B (0.24), and Fi/B (0.17). and negative correlations with B (-0.24), C/B (-0.19), and CCl/B (-0.05). In the same way, the Spearman matrix shows positive correlations with W/B (0.30), Co/B (0.29), and FiA/B (0.29), and negative correlations with B (-0.34), FA/B (-0.23), and C/B (-0.28).

**Table 1**
Statistical intuitions into the parameters.

| Statistics | B (kg/m$^3$) | W/B | C/B | FA/B | GGBF/B | SF/B | LP/B | CCl/B | CoA/B | FiA/B | SP/B | TV |
|---|---|---|---|---|---|---|---|---|---|---|---|---|
| **Carbonation rate (mm/year$^{0.5}$)** | | | | | | | | | | | | |
| **Mean** | 363.02 | 0.49 | 0.72 | 0.12 | 0.14 | 0.00 | 0.01 | 0.01 | 2.86 | 2.47 | 0.00 | 4.80 |
| **Median** | 350.00 | 0.50 | 0.74 | 0.00 | 0.00 | 0.00 | 0.00 | 0.00 | 2.74 | 2.25 | 0.00 | 4.02 |
| **Mode** | 400.00 | 0.50 | 1.00 | 0.00 | 0.00 | 0.00 | 0.00 | 0.00 | 2.45 | 4.02 | 0.00 | 4.00 |
| **SD** | 75.34 | 0.10 | 0.23 | 0.17 | 0.23 | 0.01 | 0.04 | 0.05 | 0.77 | 0.82 | 0.00 | 4.07 |
| **Maximum** | 635.00 | 0.70 | 1.00 | 0.70 | 0.85 | 0.10 | 0.25 | 0.40 | 5.32 | 4.73 | 0.03 | 40.27 |
| **Minimum** | 204.00 | 0.25 | 0.15 | 0.00 | 0.00 | 0.00 | 0.00 | 0.00 | 1.50 | 1.18 | 0.00 | 0.01 |
| **Skewness** | 0.51 | −0.04 | −0.47 | 1.25 | 1.37 | 13.38 | 3.97 | 5.60 | 0.76 | 0.65 | 2.12 | 3.17 |
| **Chloride penetration (Coulomb)** | | | | | | | | | | | | |
| **Mean** | 405.37 | 0.44 | 0.68 | 0.21 | 0.08 | 0.02 | 0.00 | 0.01 | 2.29 | 2.08 | 0.00 | 2121.58 |
| **Median** | 400.00 | 0.40 | 0.70 | 0.15 | 0.00 | 0.00 | 0.00 | 0.00 | 2.36 | 1.96 | 0.00 | 1456.00 |
| **Mode** | 400.00 | 0.40 | 1.00 | 0.00 | 0.00 | 0.00 | 0.00 | 0.00 | 0.00 | 1.87 | 0.00 | 1000.00 |
| **SD** | 82.09 | 0.11 | 0.27 | 0.24 | 0.19 | 0.04 | 0.02 | 0.04 | 1.15 | 0.58 | 0.01 | 1780.06 |
| **Maximum** | 600.00 | 0.80 | 1.00 | 0.90 | 0.90 | 0.20 | 0.20 | 0.30 | 5.04 | 6.19 | 0.03 | 13226.0 |
| **Minimum** | 237.00 | 0.25 | 0.00 | 0.00 | 0.00 | 0.00 | 0.00 | 0.00 | 0.00 | 0.99 | 0.00 | 100.00 |
| **Skewness** | 0.27 | 1.15 | −0.55 | 0.86 | 2.53 | 1.70 | 8.64 | 6.33 | −0.20 | 2.48 | 1.52 | 1.74 |

SD: Standard deviation.

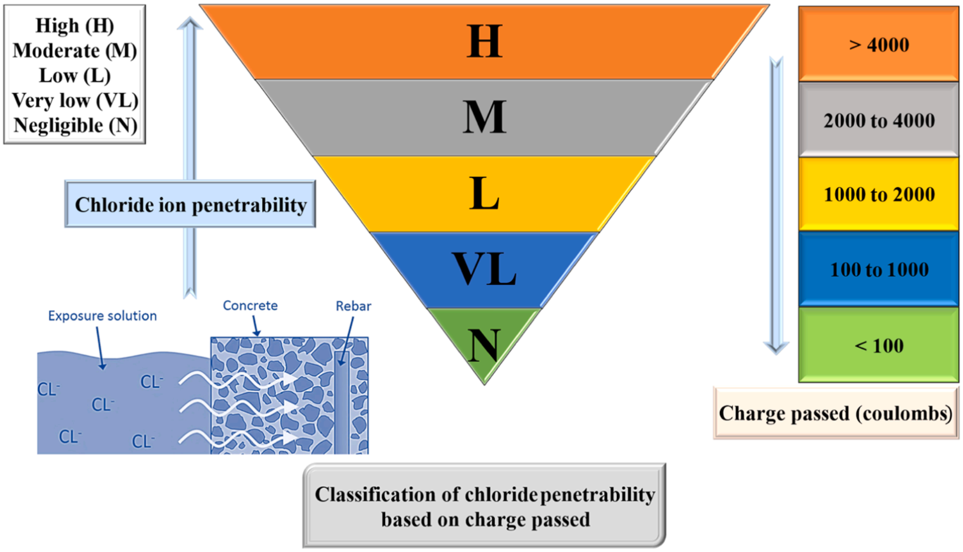


**Fig. 6.** Chloride penetrability based on charge passed.

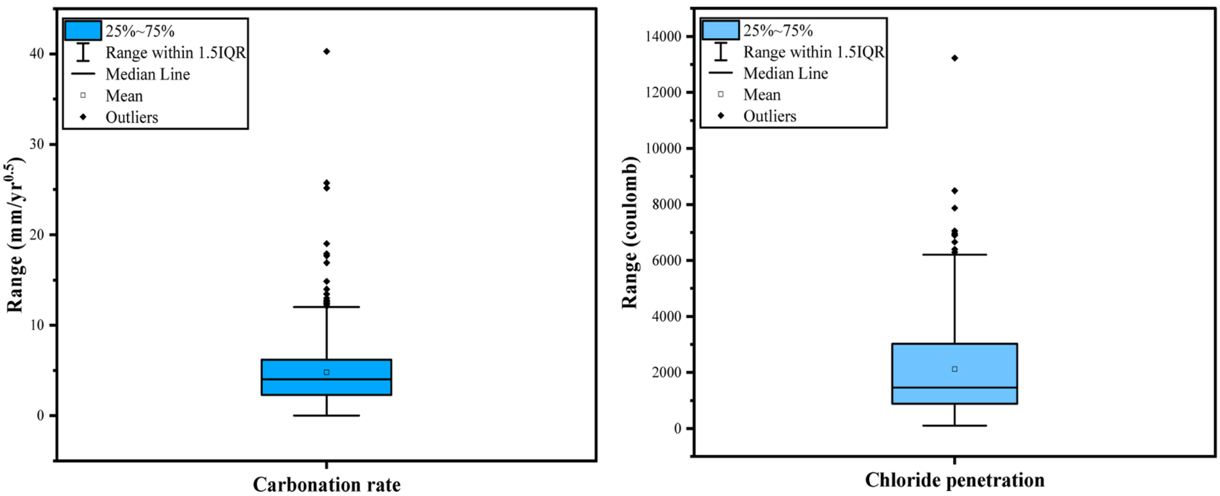


**Fig. 7.** Box plots of response variables.

### 3.2. Preprocessing of data

In data preprocessing, the main goal is to ensure data integrity by fixing errors and removing duplicates. A key step in this process is data transformation, particularly standardization, which adjusts the scales of different variables to prevent bias in machine learning models [161]. In this study, we used the StandardScaler method to standardize the dataset [162,163]. This method centers the data around the mean and scales each feature to have a unit variance [164,165]. By applying StandardScaler, the data is transformed to a common scale, reducing bias and enhancing model accuracy [166]. Standardization is especially important for models sensitive to feature scaling, such as those using distance metrics or gradient-based methods, as it ensures that all features are treated equally, leading to more reliable and accurate predictions [167–169]. Furthermore, box plots were used to identify and remove outliers, ensuring data's integrity and accuracy.

### 3.3. Model development

The process flow of model development is depicted in Fig. 9. The GEP algorithm was utilized with GeneXpro tool version 5.0, renowned for its strong data processing abilities, including efficient handling of missing values. This versatile tool can create several models from different datasets and supports code generation in several programming languages [170,171]. The general parameters include 4 genes, a head size of 10, and 1000 chromosomes, with a linking function of multiplication. The function set comprises $+$ , $-$,

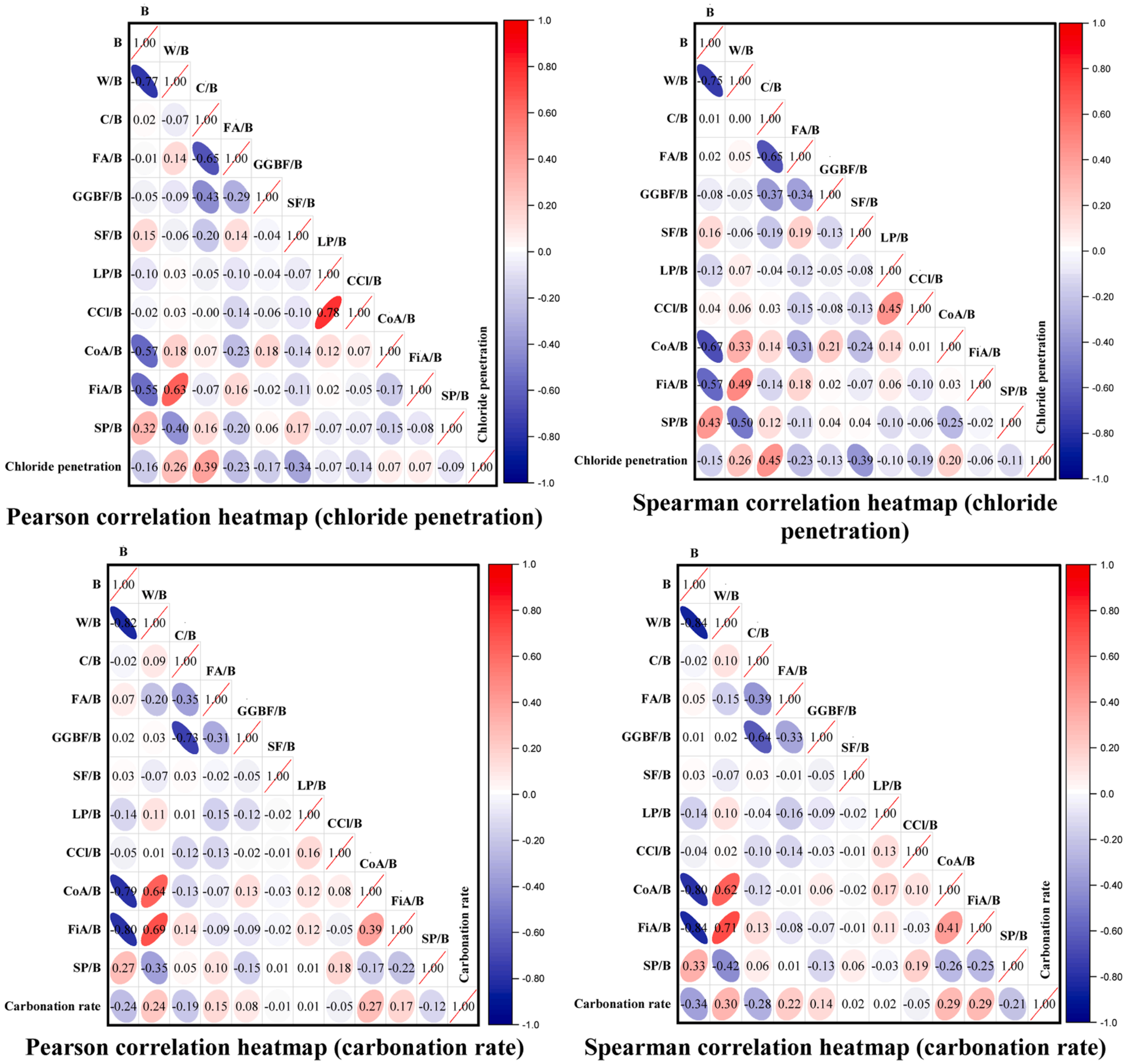


**Fig. 8.** Correlation heatmaps.

*, /, Inv, Ln, Exp, $x^2$, $x^3$, $x^4$, $x^5$, $\sqrt[3]{}$, and $\sqrt[6]{}$. For numerical constants, each gene contains 10 constants, with a floating-point data type ranging from an upper bound of 10 to a lower bound of −10. The genetic operators are set with a mutation rate of 0.00138, permutation rate of 0.00546, inversion rate of 0.00546, IS transportation rate of 0.00546, random cloning rate of 0.00102, RIS transportation rate of 0.00546, gene transportation rate of 0.00277, recombination rate of 0.00277, RNC mutation rate of 0.00206, and Dc mutation rate of 0.00206. These parameters were carefully chosen to enhance the performance and accuracy of the GEP model.

In MEP modeling, providing several setup parameters is essential to create an efficient model. These parameters were set up following suggestions and after several initial tests. The population size, which dictates the quantity of generated programs, significantly impacts the model's complexity and accuracy. A larger size of population generally leads to a more intricate and robust model, but it also increases the convergence time. However, increasing the population size beyond a certain limit can result in model overfitting [169]. The MEP model consists of 50 subpopulations, each with a size of 250, and a code length of 50. The tournament size is set to 2, with a function probability of 0.5. The mutation probability is 0.01, while the crossover probability is 0.9, and the variable probability is 0.5. The functions used in the model include addition (+), subtraction (−), multiplication (*), division (/), power (Power), square root (Sqrt), exponential (Exp), power of 10 (Pow10), sine (Sin), cosine (Cos), inverse (Inv, 1/x), arccosine (ACos), arctangent (Atan), tangent (Tan), and arcsine (ASin). These settings were carefully chosen to optimize the development and performance of the MEP model. Fig. 10 shows the convergence fitness curve, a graphical tool that illustrates the performance of optimization algorithms over successive iterations. The curve displays iterations on the x-axis and average fitness on the y-axis, demonstrating how

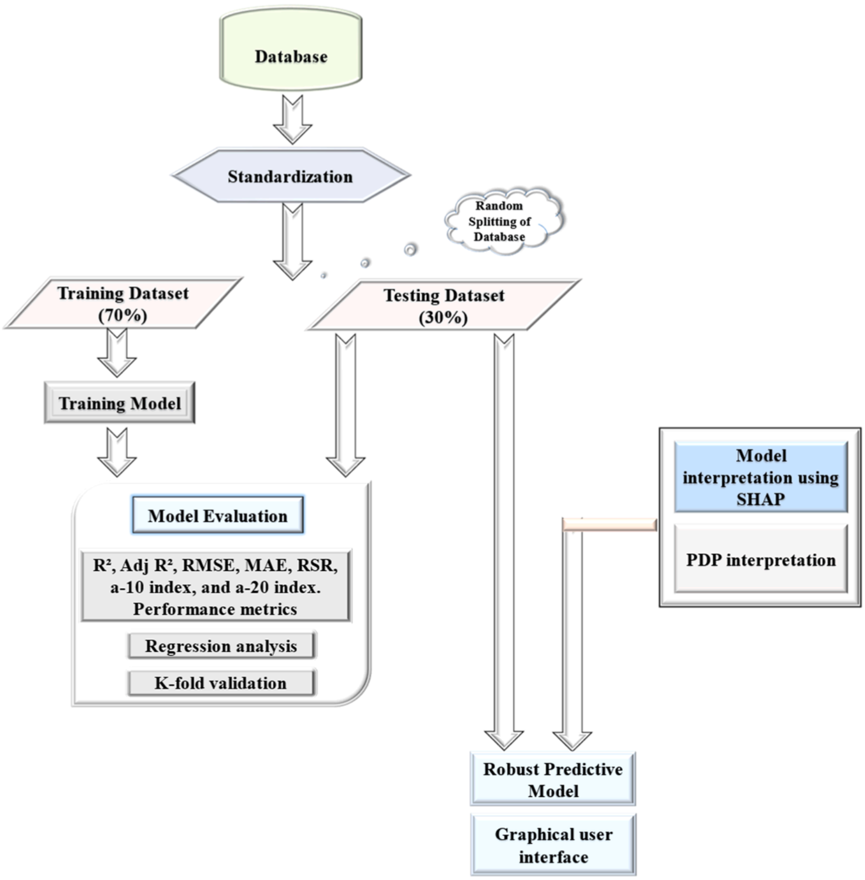


**Fig. 9.** Model development.

the algorithm progressively enhances solution quality as it converges toward an optimal result. This visualization provides valuable insights into the algorithm's convergence dynamics, allowing for the assessment of its efficiency and stability throughout the optimization process.

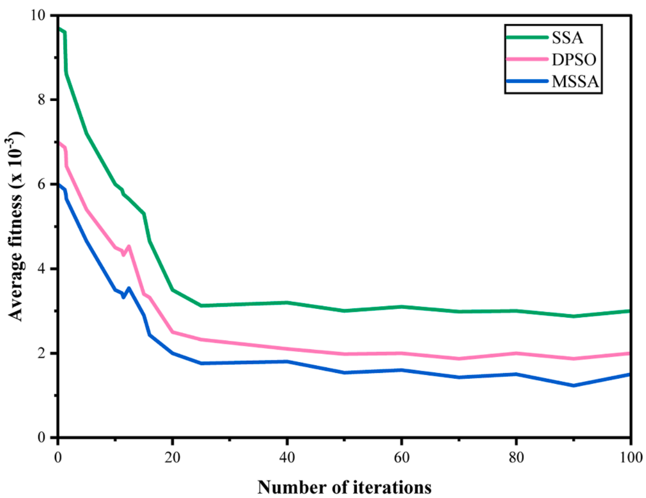


**Fig. 10.** Convergence fitness curve.

## 3.4. Evaluation of model effectiveness

### 3.4.1. Statistical assessment

Each model undergoes a comprehensive evaluation process, which includes assessing various performance metrics to thoroughly assess its reliability and effectiveness. These metrics encompass a wide range of statistical measures like the coefficient of determination ($R^2$), adjusted $R^2$ (Adj $R^2$), root mean square error (RMSE), mean absolute error (MAE), and root mean square error to observation's standard deviation ratio (RSR), along with engineering indices like the a10-index and a20-index. These metrics collectively provide valuable insights into the model's predictive capability under different conditions. By comparing the model's estimations against specific error thresholds, this evaluation ensures a robust assessment of its performance across diverse scenarios. The mathematical formulations of these metrics are presented in Eqs. 1 to 7.

$$R^2 = \frac{\left[\sum_{i=1}^{i=n}(G_i - \overline{G}_i)(H_i - \overline{H}_i)\right]^2}{\sum_{i=1}^{i=n}(G_i - \overline{G}_i)^2 \sum_{i=1}^{i=n}(H_i - \overline{H}_i)^2} \tag{1}$$

$$\text{Adj } R^2 = 1 - \frac{(1 - R^2)(N - 1)}{N - K_n - 1} \tag{2}$$

$$RMSE = \sqrt{\frac{1}{N}\sum_{i=1}^{i=n}(G_i - H_i)^2} \tag{3}$$

$$MAE = \frac{1}{N}\sum_{i=1}^{i=n}|G_i - H_i| \tag{4}$$

$$RSR = \frac{RMSE}{SD} \tag{5}$$

$$a10\_index = \frac{M10}{N} \tag{6}$$

$$a20\_index = \frac{M20}{N} \tag{7}$$

Where $G_i$ depicts the experimental value and $H_i$ showcases the estimated value for the $i^{th}$ observation, with N stands for the entire count of observations, $\overline{H}_i$ represents the mean average of the actual values, and $K_m$ shows the quantity of independent parameters. The terms M20 and M10 stand for the expected quantities of values falling within certain ranges of the experimental-to-model estimated value ratio. M20 refers to values within the range of 0.90–1.20, whereas M10 pertains to values within the range of 0.80–1.10.

### 3.4.2. K-fold cross-validation

K-fold cross-validation (kfcv) is a widely adopted method for evaluating the performance and generalizability of ML models. This technique is particularly beneficial for assessing how well a model will perform on unseen data, thus providing a reliable estimate of its

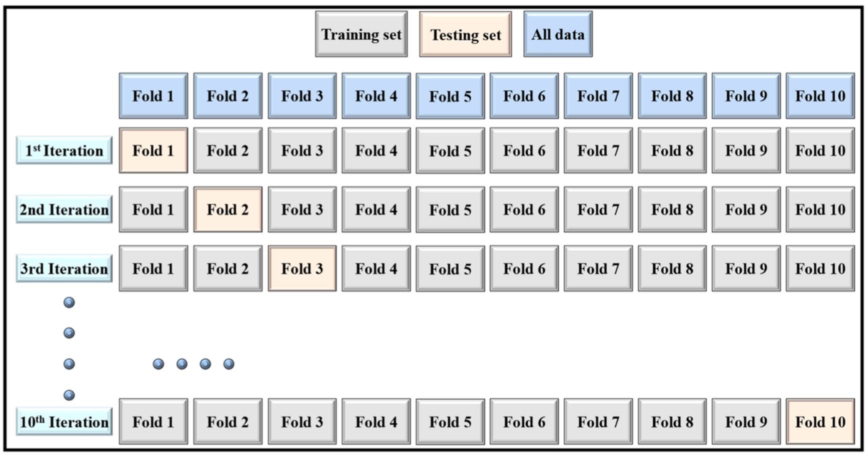


**Fig. 11.** 10-fold cross-validation.

effectiveness on an independent dataset [107]. By systematically partitioning data into k subsets and alternately using each subset for testing while training on the remaining data, kfcv effectively reduces sampling bias and mitigates the risk of overfitting. This approach minimizes the impact of any single, possibly unrepresentative, split by ensuring that the model is tested on multiple data subsets, thus yielding a more reliable performance assessment [108]. In this study, a 10-fold cross-validation was implemented, as shown in Fig. 11. The dataset was randomized and divided into ten equal parts; in each cycle, nine subsets (90 %) were used for training, while one subset (10 %) served for testing. This process was repeated across all folds, and the model's overall performance was determined by averaging the accuracy scores across the ten iterations. This method not only ensures a balanced evaluation by reducing variance and potential biases but also enhances computational efficiency, making it an effective approach for robust model assessment.

### *3.5. SHapely additive exPlanations (SHAP)*

In addition to attaining high levels of accuracy, understanding the logic behind a model's estimations is crucial across various implementations [172–174]. Developing precise ML models using extensive datasets requires the application of complex and advanced methodologies, which include both traditional machine learning and deep learning techniques. Even experienced practitioners often find it challenging to explain the underlying logic of the predictive outcomes [160]. SHAP, grounded in cooperative game theory, examines the mechanics of Shapley values, offering a systematic approach in machine learning for the detailed interpretation of individual predictions [175]. SHAP introduces a distinct set of metrics to evaluate the significance of additional features [176,177]. Theoretical insights indicate the presence of a unique solution within this metric category, showcasing favorable properties [178]. Analyzing SHAP values allows for identifying the attributes with the greatest influence on the estimations of model and understanding their interactions. This examination aids in interpreting and validating the model's behavior, pinpointing areas for potential improvement or optimization [177].

## 4. Results and discussions

### *4.1. Mathematical formulations*

Using expression trees, simplified mathematical expressions (**Equations 8 and 9**) were developed to predict the carbonation rate and chloride penetration in blended cement concrete. These empirical formulations, based on GEP, provide accurate estimates of these parameters.

$$\text{Chloride penetration} = A + B + C^2 + D \quad (8)$$

Where,

$$A = \frac{\frac{LP}{B}-9.96}{\frac{W}{B}} - e^{\frac{FiA}{B}} - B * \frac{CCl}{B}\left(\frac{C}{B} + 9.96\right)-9.94$$

$$B = \frac{C}{B}\left(2.76-\frac{W}{B}\right)\left(\frac{SF}{B} * B + 10.97\right)\left(-9.78*\frac{FiA}{B}\right)$$

$$C = \frac{C}{B} * \frac{e^{W/B}}{\frac{Cl}{B}+\frac{W}{B}} * \left(\frac{FiA}{B} + 9.42\right)\left(3.09*\frac{W}{B}\right)$$

$$D = \frac{W}{B} + 6.58 + 10.36*\left(\frac{FA}{B}\right)^2\left(\frac{2.44}{6.42*\frac{FiA}{B}}\right)$$

$$\text{Carbonation rate} = E + F + G + H + I^2 \quad (9)$$

Where,

$$E = \mathrm{Tanh}\left(\left(\frac{FA}{B} + \frac{W}{B} * \frac{SP}{B} + \frac{LP}{B} * \frac{CCl}{B}\right) * 1142\right)$$

$$F = \mathrm{Tanh}\left(-2.9 + 10.89*\frac{LP}{B} + 9.35*\frac{FA}{B} * \frac{CoA}{B}\right)$$

$$G = 2.89*\left(\frac{W}{B}\right)^3 * \left(\frac{CoA}{B} + 2.38\right)$$

$$H = \frac{CoA}{B} + \frac{CoA}{B} * \left(\left(-9.43 + \frac{CoA}{B}\right)\left(-5.57*\frac{SP}{B}\right)\right)^3$$

$$I = \left(\frac{GGBF}{B}\right)^{\frac{1}{2}}\left(\frac{-2.5}{\frac{CoA}{B}}-3.14 + \frac{CoA}{B} - \frac{FA}{B} * \frac{CoA}{B}\right)$$

### 4.2. Regression analysis

The regression slopes (Fig. 12) for the GEP and MEP models were analyzed to evaluate their predictive accuracy for chloride penetration and carbonation rate in concrete. For chloride penetration, the GEP model demonstrated a regression slope of 0.91 during the training phase and 0.96 during the testing phase. In comparison, the MEP model exhibited regression slopes of 0.85 and 0.94 for the training and testing phases, respectively, which are slightly lower than those of the GEP model. For the carbonation rate, the GEP model again demonstrated higher regression slopes with scores of 0.91 during the training phase and 0.87 during the testing phase as shown in Fig. 10. The MEP model had regression slopes of 0.82 for the training phase and 0.83 for the testing phase. These results indicate that the GEP model maintains a closer fit to the actual data compared to the MEP model in both training and testing phases for both chloride penetration and carbonation rate. Overall, the higher regression slopes achieved by the GEP model in both phases for both parameters further underscore its superior performance and reliability in estimating the durability characteristics of BCC compared to the MEP model.

### 4.3. Evaluation of model effectiveness

#### 4.3.1. Statistical assessment

The effectiveness of GEP and MEP models was evaluated for predicting carbonation rate and chloride penetration in concrete as presented in Table 2. For the carbonation rate, the GEP model surpassed the MEP model in both training and testing phases. Specifically, the GEP model attained an $R^2$ of 0.978 and an adjusted $R^2$ of 0.977 in the training set, compared to the MEP model's $R^2$ of 0.919 and adjusted $R^2$ of 0.972. The GEP model also had lower values for RMSE (0.487), MAE (0.282), and RSR (0.164), and higher a-10 (0.739) and a-20 (0.870) indices, indicating superior predictive accuracy and precision. In the testing phase, the GEP model maintained its superior performance with an $R^2$ of 0.954, adjusted $R^2$ of 0.951, RMSE of 1.050, MAE of 0.252, and an RSR of 0.180,

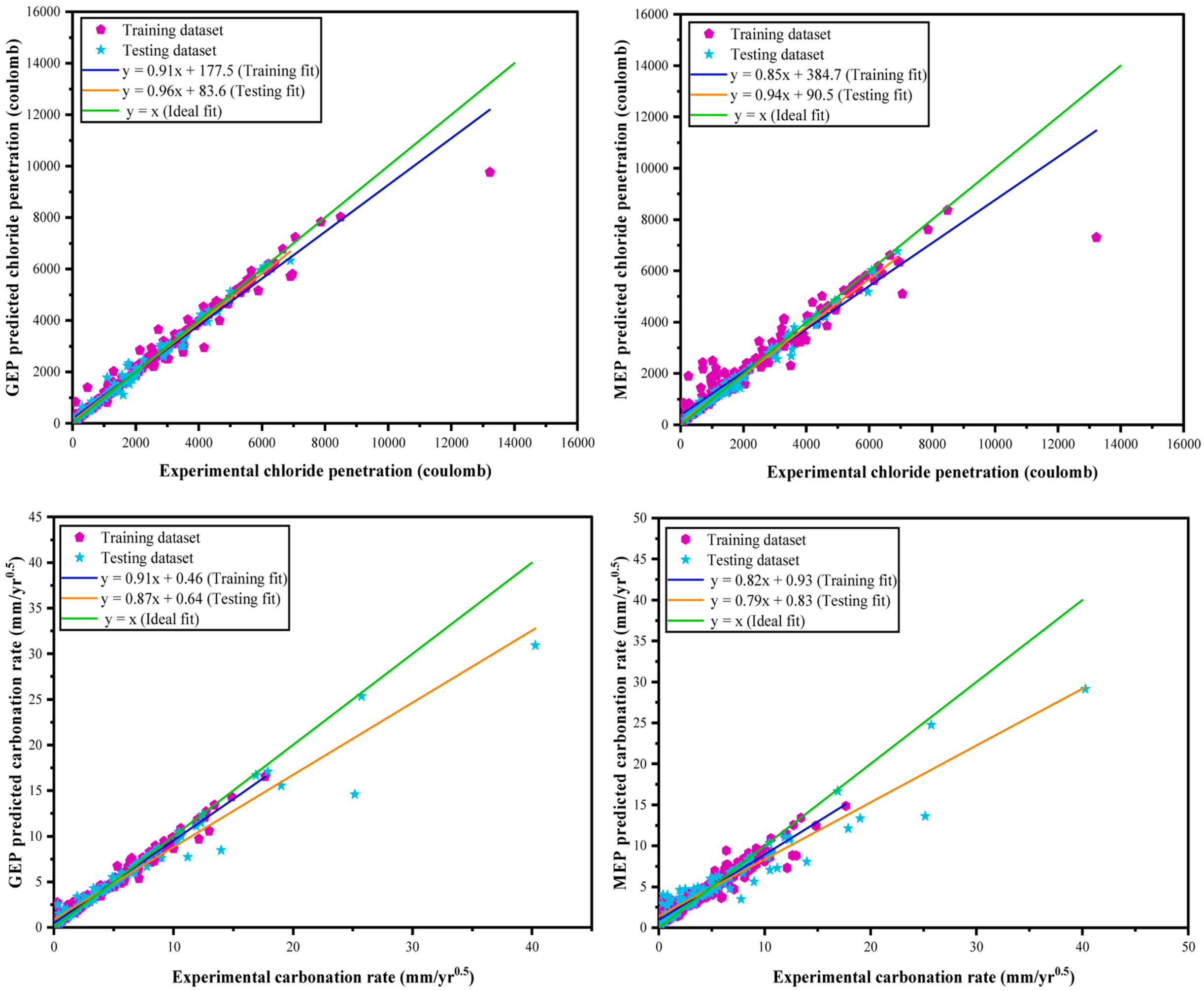


**Fig. 12.** Regression analysis.

**Table 2**
Performance summary of statistical indicators.

| Set | Model | $R^2$ | Adj $R^2$ | RMSE | MAE | RSR | a-10 index | a-20 index |
|---|---|---|---|---|---|---|---|---|
| Carbonation rate | | | | | | | | |
| Training | MEP | 0.919 | 0.972 | 0.921 | 0.584 | 0.310 | 0.522 | 0.731 |
| | GEP | 0.978 | 0.977 | 0.487 | 0.282 | 0.164 | 0.739 | 0.870 |
| Testing | MEP | 0.913 | 0.910 | 1.434 | 0.489 | 0.246 | 0.418 | 0.664 |
| | GEP | 0.954 | 0.951 | 1.050 | 0.252 | 0.180 | 0.682 | 0.800 |
| Chloride penetration | | | | | | | | |
| Training | MEP | 0.924 | 0.921 | 0.957 | 0.950 | 0.166 | 0.680 | 0.890 |
| | GEP | 0.973 | 0.971 | 0.505 | 0.830 | 0.015 | 0.840 | 0.920 |
| Testing | MEP | 0.985 | 0.984 | 1.440 | 0.560 | 0.340 | 0.694 | 0.847 |
| | GEP | 0.990 | 0.990 | 1.100 | 0.230 | 0.230 | 0.745 | 0.867 |

along with higher a-10 (0.682) and a-20 (0.800) indices, compared to the MEP model's $R^2$ of 0.913, adjusted $R^2$ of 0.910, RMSE of 1.434, MAE of 0.489, and RSR of 0.246, and a-10 (0.418) and a-20 (0.664) indices.

Similarly, for chloride penetration, the GEP model again demonstrated superior performance over the MEP model. In the training phase, the GEP model achieved an $R^2$ of 0.973, adjusted $R^2$ of 0.971, RMSE of 0.505, MAE of 0.830, and RSR of 0.015, with a-10 (0.840) and a-20 (0.920) indices, whereas the MEP model showed an $R^2$ of 0.924, adjusted $R^2$ of 0.921, RMSE of 0.957, MAE of 0.950, and RSR of 0.166, with a-10 (0.680) and a-20 (0.890) indices. In the testing phase, the GEP model sustained its lead with an $R^2$ of 0.990,

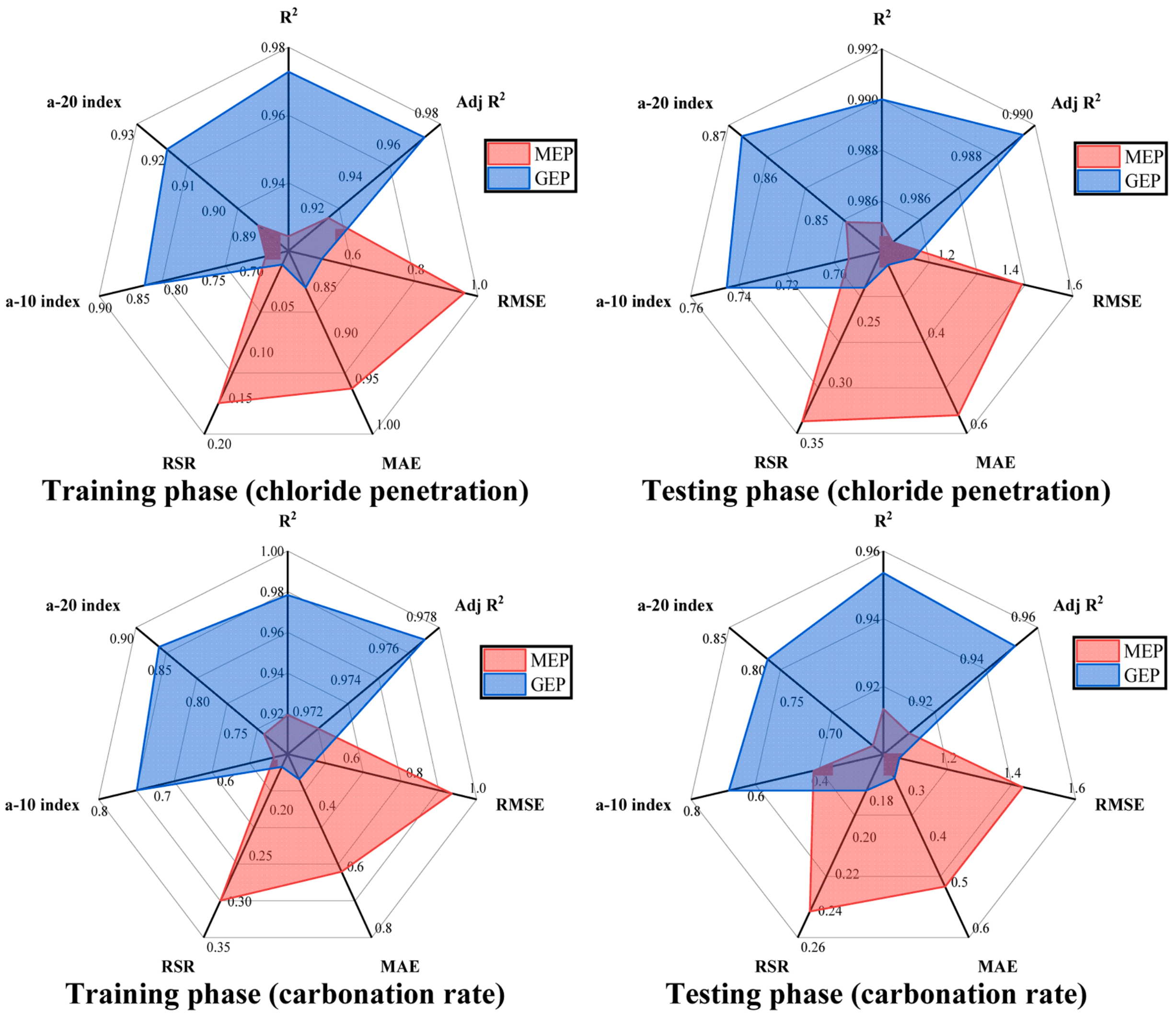


**Fig. 13.** Spider plots of statistical indicators.

adjusted $R^2$ of 0.990, RMSE of 1.100, MAE of 0.230, and RSR of 0.230, with a-10 (0.745) and a-20 (0.867) indices, compared to the MEP model's $R^2$ of 0.985, adjusted $R^2$ of 0.984, RMSE of 1.440, MAE of 0.560, and RSR of 0.340, and a-10 (0.694) and a-20 (0.847) indices.

Overall, the GEP model consistently demonstrated superior results compared the MEP model across all statistical indicators for both carbonation rate and chloride penetration, making it the preferred choice for predicting these parameters in blended cement concrete. Spider plots of statistical indicators are depicted in Fig. 13.

#### 4.3.2. K-fold cross-validation

In this study, a 10-fold cross-validation was implemented, as shown in Figs. 14 and 15. The dataset was randomized and divided into ten equal parts; in each cycle, nine subsets (90 %) were used for training, while one subset (10 %) served for testing. This process was repeated across all folds, and the model's overall performance was determined by averaging the accuracy scores across the ten iterations. Both GEP and MEP models demonstrated strong performance. For carbonation rate prediction, GEP achieved an average $R^2$ of 0.962 and an RMSE of 0.829, while MEP achieved an average $R^2$ of 0.932 and an RMSE of 1.143. For chloride penetration prediction, GEP achieved an average $R^2$ of 0.965 and an RMSE of 0.858, whereas MEP achieved an average $R^2$ of 0.931 and an RMSE of 1.247.

### 4.4. SHAP interpretation

#### 4.4.1. Mean SHAP plots

Mean SHAP plots are showcased in Fig. 16. The SHAP scores for chloride penetration and carbonation rate reveal significant intuitions into the impact of various features on the model's estimations. For chloride penetration, C/B stands out with the highest mean SHAP value of approximately 800, indicating its dominant role in affecting the model output. The SF/B follows with a mean SHAP value of around 370, and W/B has a mean SHAP value of approximately 280. The CoA/B, Binder, FA/B, and FiA/B each have mean SHAP values of around 180, suggesting their moderate impact. The SP/B has a mean SHAP value of around 120, and the GGBF/B has a mean SHAP score of around 30, indicating a lesser influence on chloride penetration. For the carbonation rate, the W/B depicts the highest mean SHAP score of around 1.4, highlighting its significant effect on the model's predictions as depicted in Fig. 16. The C/B has a mean SHAP value of approximately 1, followed by the FA/B with a mean SHAP value of around 0.8. The CoA/B has a mean SHAP value of around 0.42, and the SP/B shows a mean SHAP value of approximately 0.35. The Binder has a substantial mean SHAP value of around 3, indicating its strong influence. Finally, the GGBF/B has a mean SHAP value of around 0.8, reflecting its moderate impact on the carbonation rate. Overall, these SHAP values emphasize the critical features driving the model's predictions for both chloride penetration and carbonation rate, with C/B and W/B ratios consistently showing high influence across both parameters. It was observed that Portland cement concretes are more susceptible to carbonation than their counterparts that incorporate limestone or pozzolanic materials [179]. After 56 days, two types of concrete, one made with Portland cement and the other with Portland-fly ash cement, exhibited a tendency to reach the maximum depth of carbonation [180].

#### 4.4.2. SHAP summary plots

SHAP summary plots are illustrated in Fig. 17. For chloride penetration, the SHAP score of the C/B rises with an increase in C/B and vice versa, showing a peak SHAP value of around 3200 and a maximum negative SHAP value of around −1800. The SHAP value of the SF/B decreases with an increase in SF/B and vice versa, with a highest SHAP value of approximately 3900 and a greatest negative SHAP value of around −1100. The SHAP value of the W/B also increases with a rise in W/B and vice versa, reaching a peak SHAP value of around 1200 and a highest negative SHAP value of about −1400. Additionally, the SHAP value of the CoA/B decreases with an

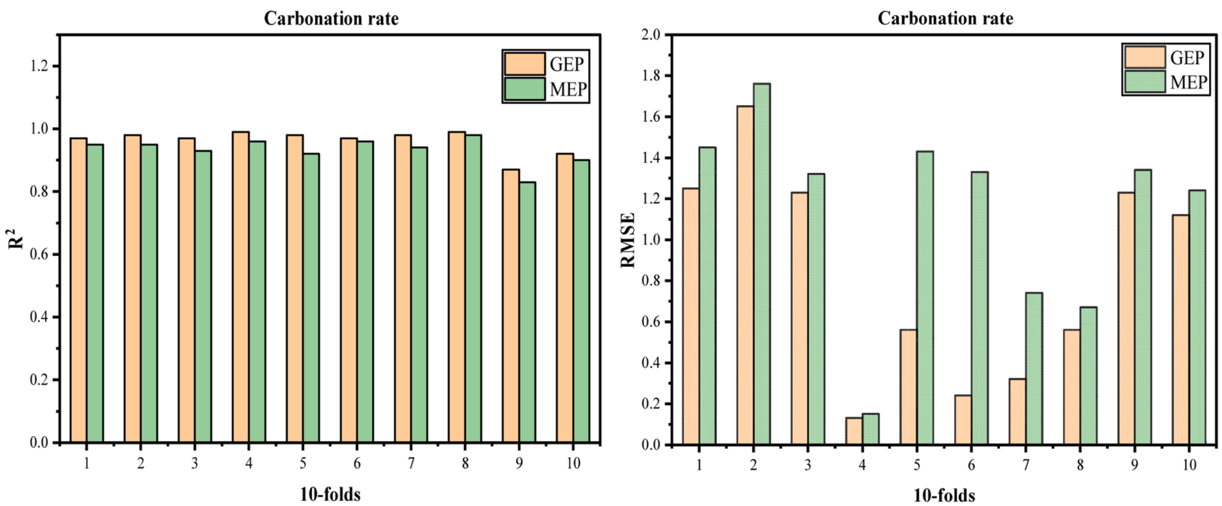


**Fig. 14.** 10-fold cross-validation of the models for carbonation rate.

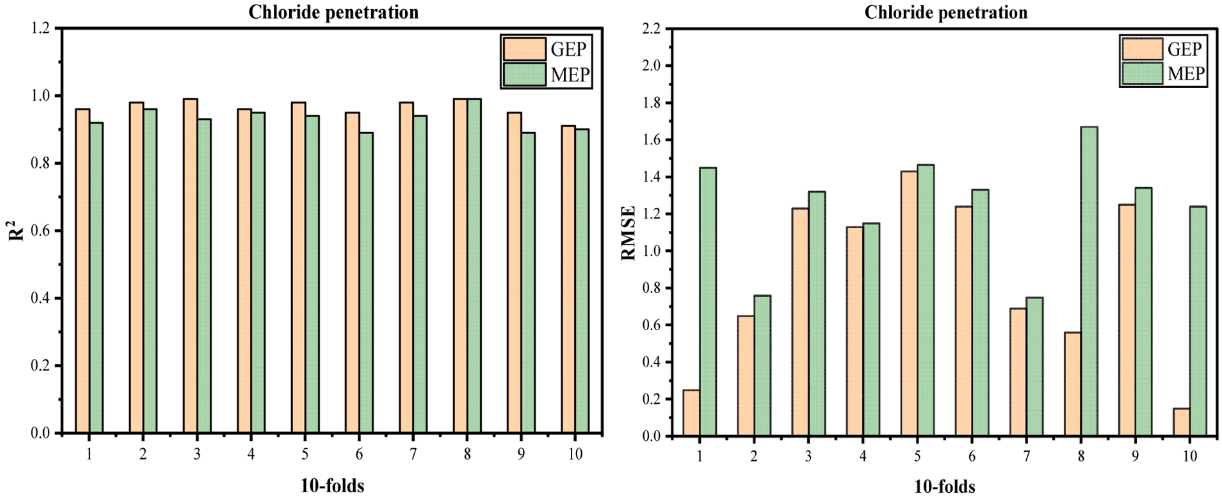


**Fig. 15.** 10-fold cross-validation of the models for chloride penetrability.

increase in CoA/B and vice versa, exhibiting a greatest SHAP value of around 2100 and a maximum negative SHAP value of approximately −900. The Binder demonstrates a similar trend, with its SHAP value decreasing as Binder increases and vice versa, showing a maximum SHAP value of around 800 and a maximum negative SHAP value of approximately −1100. The SHAP score of the FA/B escalates with a rise in FA/B and vice versa, reaching a maximum SHAP value of about 1900 and a maximum negative SHAP value of around −300. Finally, the SHAP value of the Fi/B decreases with an increase in FiA/B and vice versa, with a maximum SHAP value of around 2000 and a maximum negative SHAP value of about −600. Polycarboxylate superplasticizers result in reduced carbonation depth, water penetration depth, and chloride permeability of concrete. This improvement is attributed to the denser microstructure they promote in the concrete [181]. In the early stages of curing, a small addition of fly ash can actually increase the chloride migration coefficient. However, a significant reduction in the coefficient is observed with a higher amount of fly ash incorporation during this period [182]. Concrete made with slag cements exhibits significantly lower chloride permeability when compared to other concrete mixtures [183]. Silica incorporation improved the resistance of concrete to chloride and sulfate attacks, as evidenced by the reduced strength loss following exposure to sulfate attack [184].

The SHAP values for the carbonation rate reveal detailed insights into how various features influence the model's predictions. The SHAP value of the W/B increases with a rise in W/B and vice versa, with a maximum SHAP value of around 25 and a maximum negative SHAP value of around −6 as depicted in Fig. 17. Conversely, the SHAP value of the C/B decreases with an increase in C/B and vice versa, showing a maximum SHAP value of approximately 4 and a maximum negative SHAP value of around −4. The FA/B exhibits a complex behavior, indicating a nuanced influence on the estimations of the model. The SHAP value of the FiA/B increases with an increase in FiA/B and vice versa, reaching a maximum SHAP value of around 3 and a maximum negative SHAP value of about −2. Similarly, the SHAP value of the CoA/B rises with an increase in CoA/B and vice versa, showing a maximum SHAP value of around 4 and a maximum negative SHAP value of approximately −2. The SP/B demonstrates a decrease in SHAP value with an increase in SP/B and vice versa, with a maximum SHAP value of around 4 and a maximum negative SHAP value of about −2.5. The Binder also shows complex behavior, indicating its varied influence on the carbonation rate. Features such as the GGBF/B, LP/B, CCI/B, and SF/B also influence the estimations of the model but to a lesser extent. Their SHAP values are relatively centered around zero, indicating a lower overall impact on the carbonation rate. The carbonation rate of the Portland cement mixture exceeded that of blended cement mixtures. Among all the mixtures tested, those with Ptolemaida treated fly ash blended cements exhibited the lowest carbonation rate [185]. When the water/binder ratio increased from 0.30 to 0.35, the $CO_2$ uptake ratio rose from 3.84 % to 5.38 % due to the greater carbonation depth and reaction level of the binders [186].

### 4.5. PDP interpretation

Understanding how functions behave with inputs in multiple dimensions can be complex. Therefore, studying the partial dependence of the estimated function on specific subsets of input variables can be advantageous. Although a collection of these plots may not completely capture the approximation, they can offer valuable insights, especially when the function is primarily influenced by lower-order interactions [187,188]. Partial dependence plots (PDP) are visual tools frequently used in machine learning to understand the relationship between predictor variables and the target variable [189]. These plots show the average predicted outcome across all data points for a specific predictor variable, taking into account the influences of other predictor variables [190].

In Fig. 18, PDPs are depicted. The trend in chloride penetration shows a relatively stable pattern as B, GGBF/B, LP/B, and CCl/B increase. However, it increases notably with higher W/B and FA/B ratios. Specifically, chloride penetration maintains a nearly constant level within the range of approximately 0.35–0.78. Beyond 0.78 and up to 0.8, there is a sharp escalation, followed by a decrease from 0.8 to around 0.98, and then another rapid increase from 0.98 to 1. Additionally, chloride penetration remains stable up to

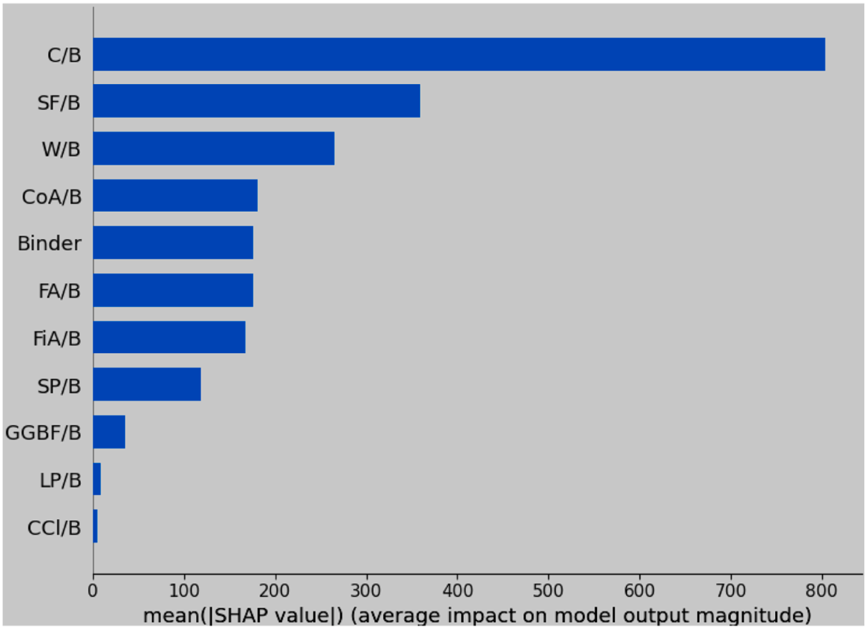


**Chloride penetration**

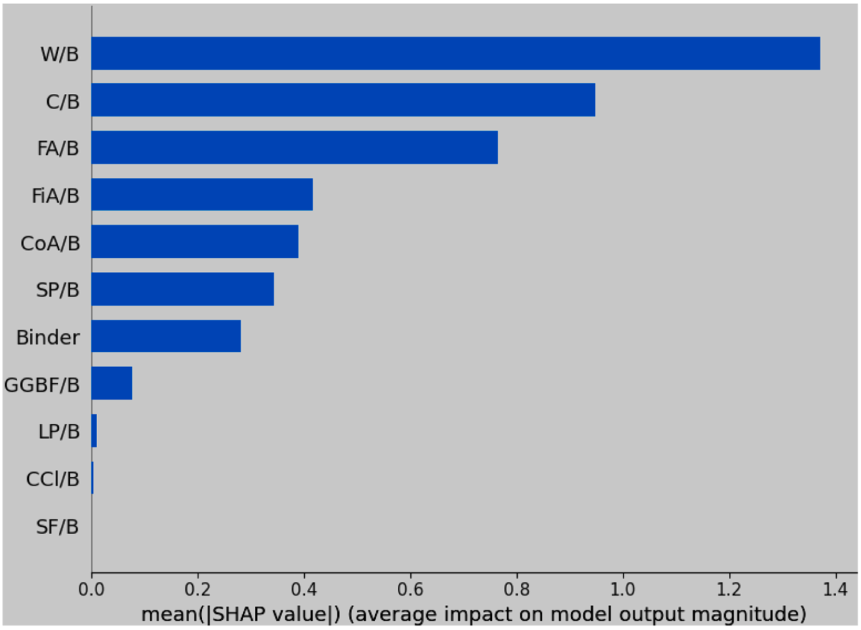


**Carbonation rate**

**Fig. 16.** Mean SHAP plots.

approximately 0.30 of SF/B, after which it experiences a steep decline until around 0.35, beyond which it stabilizes again. Notably, chloride penetration exhibits a complex relationship with CoA/B. It increases as Fi/B rises, particularly showing a rapid surge from 2.75 to about 2.9. Conversely, it decreases as SP/B increases, maintaining stability beyond a ratio of 1. The utilization of fly ash decreased the chloride permeability of the concrete [183]. Blended cement concrete mixtures demonstrate significantly improved resistance to chloride ion penetration and reduced risk of reinforcement corrosion compared to plain Portland cement concrete mixtures [191]. An increase in the water-to-cement ratio leads to a greater depth of chloride penetration, all other factors being equal [192].

The rate of carbonation exhibits a relatively stable trend with increasing GGBF/B, SF/B, LP/B, and CCl/B ratios (Fig. 18). However, it shows a slight decrease with an increase in B, with a rise observed from 350 to 390. Furthermore, the carbonation rate decreases as W/B increases, with a notable increase noted from 0.55 to 0.65. Similarly, there is a decreasing trend in the carbonation rate with

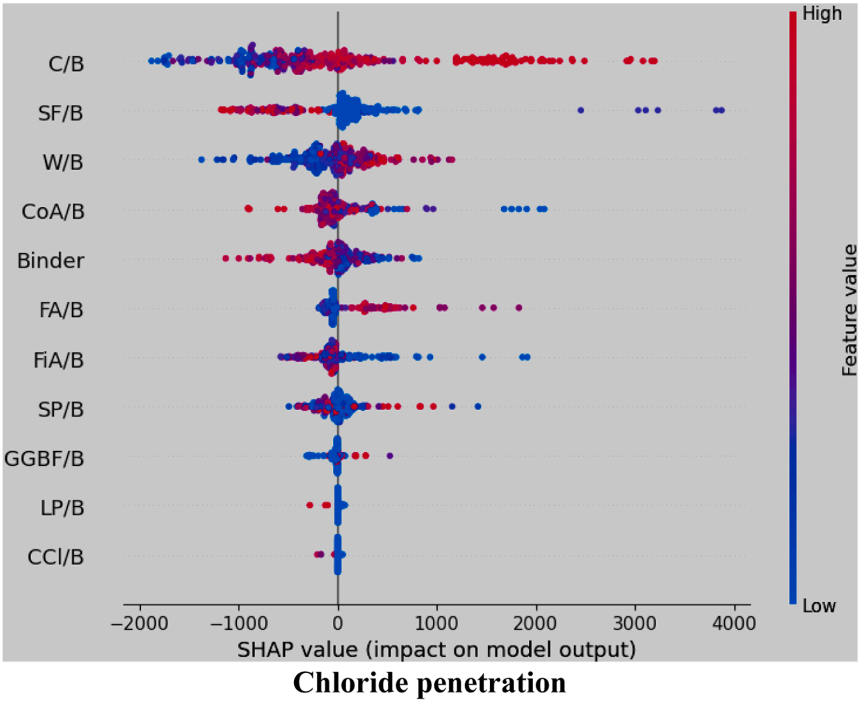


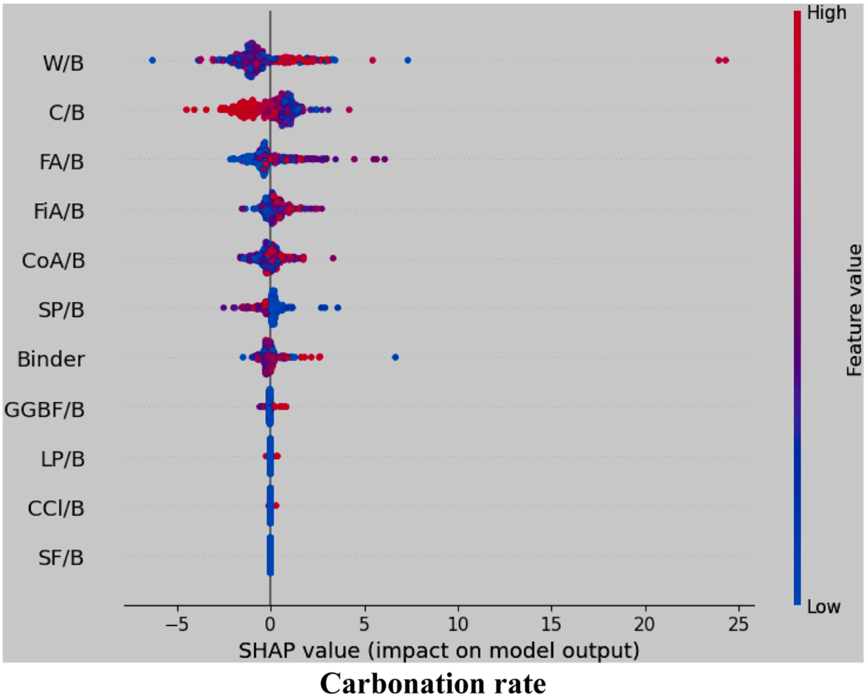


**Fig. 17.** SHAP summary plots.

higher C/B ratios. Interestingly, the carbonation rate initially increases with an increase in FA/B, reaching a peak around 0.26, then decreases until approximately 0.32, and stabilizes thereafter. Regarding Co/B, the carbonation rate decreases initially, reaching a minimum around 2.8, then rises until about 3.25 before decreasing again. It also shows an increasing trend with higher Fi/B ratios. Conversely, the carbonation rate decreases initially with an increase in SP/B up to around 0.0065, beyond which it starts to increase. The addition of 10 % silica fume and 0.07 % propylene short fibers by volumetric fraction effectively reduced carbonation depth [193]. An increase in the W/B ratio resulted in higher CO2 uptake [186]. It has demonstrated that combining pulverized coal

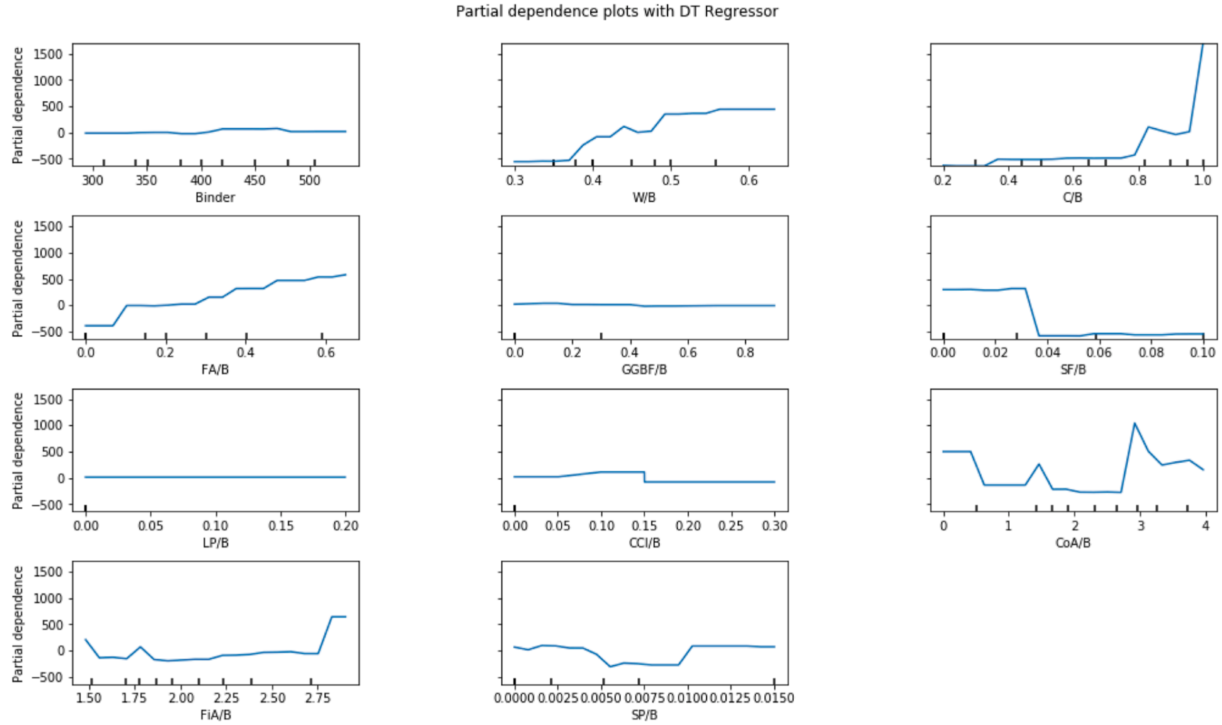


**Chloride penetration**

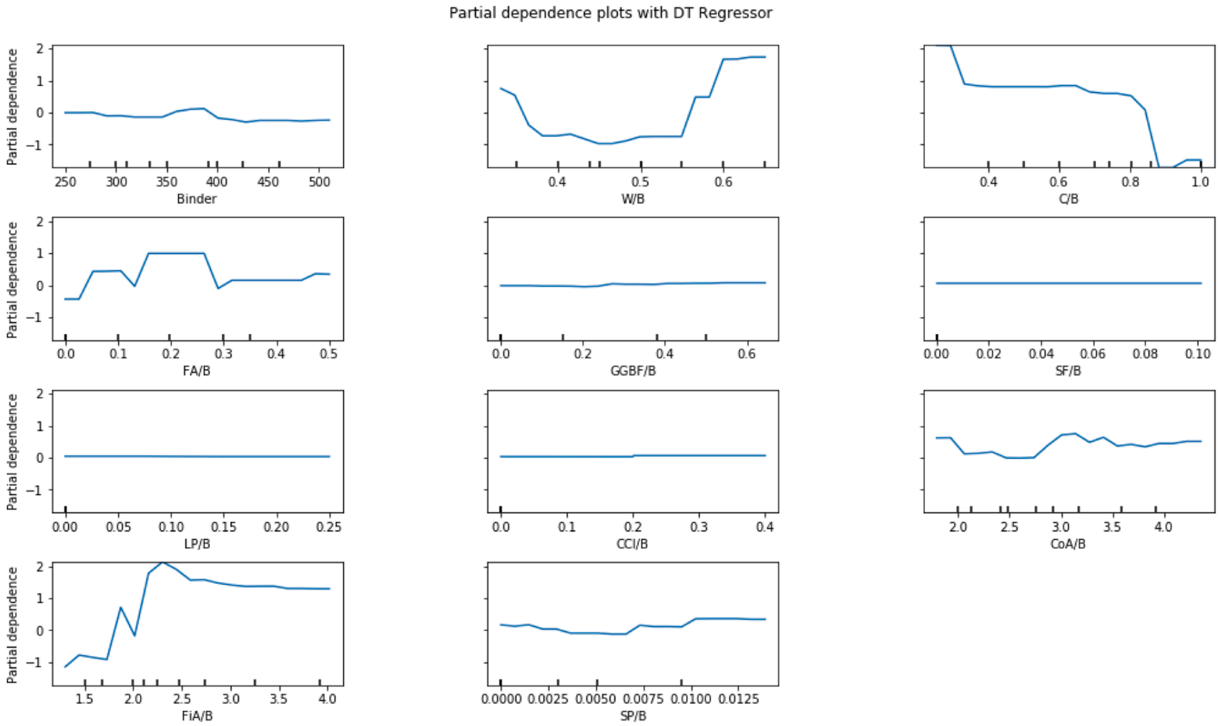


**Carbonation rate**

**Fig. 18.** PDPs.

combustion ash with circulating fluidized bed combustion ash enhances the CO2 sequestration properties of belite-rich cement [194].

## 5. Graphical user interface

A user-friendly graphical interface (GUI), illustrated in Fig. 19, was developed to simplify predicting the durability characteristics of BCC. This tool significantly improves the efficiency of strength estimation by removing the need for traditional, labor-intensive, and time-consuming laboratory tests. Users can input relevant parameters to quickly generate accurate predictions of carbonation rates and chloride penetrability. Utilizing advanced machine learning algorithms, this interface provides a practical and accessible solution for researchers and industry professionals to assess durability performance without requiring physical testing.

## 6. Limitations of the study and research directions for future

The dataset utilized for this study included 362 experimental data sets for carbonation rate and 326 for chloride penetration, gathered from various literature sources. However, this dataset size is relatively small for developing a robust machine learning model. Increasing the dataset is crucial for improving the model's accuracy. A larger and more diverse dataset would provide the model with more comprehensive information, enhancing its ability to generalize and perform better in predictions. Additionally, it is important to highlight that the data for this study was sourced from existing literature. The experimental conditions across these studies varied widely, resulting in a dataset with limited diversity. To develop more reliable models, it is crucial to conduct controlled experiments under consistent conditions and gather data from a single, unified source that accurately reflects real-world environmental scenarios. This approach would enhance the dataset's uniformity and relevance, thereby improving the robustness and applicability of the machine learning models. Furthermore, gene expression programming could be employed to develop empirical formulae for predicting the chloride penetration and carbonation rate of blended cement concrete. This approach would enable the derivation of precise mathematical models that account for the complex interactions between various factors affecting these properties. Moreover, it is worth noting that the exploration of hybrid models and machine learning models optimized using advanced optimization algorithms could be a valuable direction for future research. Integrating these sophisticated techniques has the potential to significantly enhance model accuracy and reliability.

## 7. Conclusions

This study employed GEP and MEP to predict the chloride penetration and carbonation rate of blended cement concrete. The database employed comprised 362 sets of experimental data for carbonation rate and 326 sets for chloride penetration, collected from various literature sources. To thoroughly assess the effectiveness of the proposed models, a range of statistical metrics including $R^2$, adj $R^2$, RMSE, MAE, RSR, a-10 index, and a-20 index were utilized. Moreover, to enhance the interpretability of model predictions, the SHAP method was utilized. Furthermore, PDP analysis was conducted to provide deeper insights. The key findings derived from this research effort are summarized below.

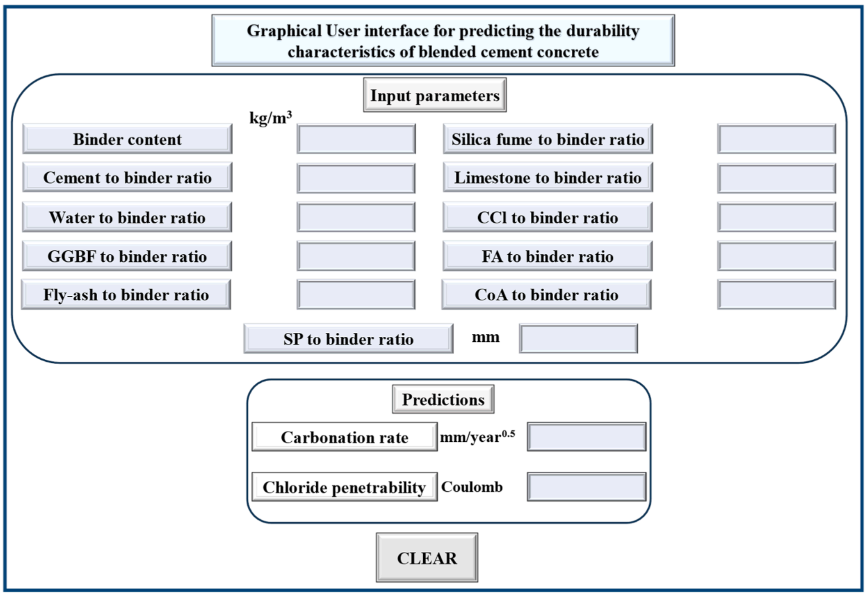


Fig. 19. GUI for forecasting the durability characteristics of BCC.

- Both GEP and MEP models consistently demonstrated superior performance across all statistical indicators for both carbonation rate and chloride penetration, making them the preferred choices for predicting these parameters in blended cement concrete. Notably, for chloride penetration, the GEP model attained a high $R^2$ score of 0.954, along with minimal MAE and RMSE values of 0.252 and 1.050, respectively. Similarly, for carbonation rate, the GEP model attained a near-perfect $R^2$ value of 0.99, with corresponding MAE and RMSE values of 0.230 and 1.100, underscoring its precision in modeling this parameter. For chloride penetration, the MEP model achieved a high $R^2$ score of 0.913, alongside minimal MAE and RMSE values of 0.489 and 1.434, respectively. Similarly, for carbonation rate, the MEP model achieved a near-perfect $R^2$ value of 0.985, with corresponding MAE and RMSE scores of 0.560 and 1.440, further highlighting its accuracy in modeling this parameter.
- The SHAP values highlight the significant impact of various parameters on the forecasts. In predicting chloride penetration, C/B emerged as the most impactful feature, followed by SF/B and W/B in terms of importance. For carbonation rate, W/B stood out as the most influential, with C/B and FA/B being the subsequent key factors. These intuitions are further supported by PDP plots.
- The SHAP summary plot clearly delineates the relationships between different parameters and the estimated characteristics. Regarding chloride penetration, there is a notable positive correlation with C/B, with W/B also displaying a positive relationship. Conversely, SF/B shows a negative impact on chloride penetration. For carbonation rate, W/B emerges as a key driver with a strong positive correlation, emphasizing its influence. FA/B also shows a positive association with the carbonation rate. However, it is notable that C/B displays a negative association with the carbonation rate.
- Mathematical equations have been developed to predict chloride penetration and carbonation resistance. Additionally, a graphical user interface is being developed to enable predictions based solely on input values, thereby eliminating the need for extensive physical testing.

## CRediT authorship contribution statement

**Javed Muhammad Faisal:** Visualization, Validation, Supervision, Software, Project administration, Methodology, Investigation, Formal analysis, Data curation, Conceptualization. **Ullah Irfan:** Writing – review & editing, Writing – original draft, Visualization, Validation, Software, Methodology, Data curation, Conceptualization. **Lei Hua:** Formal analysis, Investigation, Resources, Validation. **El-Meligy Mohammed:** Data curation, Formal analysis, Investigation, Methodology. **Fu Bo:** Formal analysis, Funding acquisition, Investigation, Resources. **Hindi Khalil El:** Formal analysis, Funding acquisition, Investigation, Methodology. **Ahmad Furqan:** Data curation, Formal analysis, Funding acquisition, Investigation, Methodology.

## Declaration of Competing Interest

The authors declare that they have no known competing financial interests or personal relationships that could have appeared to influence the work reported in this paper.

## Acknowledgements

The authors extend their appreciation to King Saud University for funding this work through Researchers Supporting Project number (RSPD2025R953), King Saud University, Riyadh, Saudi Arabia.

## Data availability

Data will be made available on request.

## References

[1] Y. Ding, J.G. Dai, C.J. Shi, Mechanical properties of alkali-activated concrete: a state-of-the-art review, Constr. Build. Mater. 127 (2016) 68–79, https://doi.org/10.1016/j.conbuildmat.2016.09.121.
[2] H. Hafez, A. Teirelbar, R. Kurda, N. Tošić, A. de la Fuente, Pre-bcc: a novel integrated machine learning framework for predicting mechanical and durability properties of blended cement concrete, Constr. Build. Mater. 352 (2022), https://doi.org/10.1016/j.conbuildmat.2022.129019.
[3] M. Khan, M.F. Javed, Towards sustainable construction: machine learning based predictive models for strength and durability characteristics of blended cement concrete, Mater. Today Commun. 37 (2023), https://doi.org/10.1016/j.mtcomm.2023.107428.
[4] Y. Liu, J. Dong, S. Yuan, K. Li, X. Hu, Q. Wang, Variable fatigue loading effects on corrugated steel box girders with recycled concrete, J. Constr. Steel Res. 215 (2024), https://doi.org/10.1016/j.jcsr.2024.108526.
[5] K.M. Anwar Hossain, High strength blended cement concrete incorporating volcanic ash: performance at high temperatures, Cem. Concr. Compos. 28 (2006) 535–545, https://doi.org/10.1016/j.cemconcomp.2006.01.013.
[6] D.A. Adesanya, A.A. Raheem, A study of the workability and compressive strength characteristics of corn cob ash blended cement concrete, Constr. Build. Mater. 23 (2009) 311–317, https://doi.org/10.1016/j.conbuildmat.2007.12.004.
[7] S.J. Kwon, H.S. Lee, S. Karthick, V. Saraswathy, H.M. Yang, Long-term corrosion performance of blended cement concrete in the marine environment – a real-time study, Constr. Build. Mater. 154 (2017) 349–360, https://doi.org/10.1016/j.conbuildmat.2017.07.237.
[8] H.E.D.H. Seleem, A.M. Rashad, T. Elsokary, Effect of elevated temperature on physico-mechanical properties of blended cement concrete, Constr. Build. Mater. 25 (2011) 1009–1017, https://doi.org/10.1016/j.conbuildmat.2010.06.078.
[9] K.M.A. Hossain, M. Lachemi, Performance of volcanic ash and pumice based blended cement concrete in mixed sulfate environment, Cem. Concr. Res. 36 (2006) 1123–1133, https://doi.org/10.1016/j.cemconres.2006.03.010.
[10] A. Vollpracht, B. Lothenbach, R. Snellings, J. Haufe, The pore solution of blended cements: a review, Mater. Struct. Constr. 49 (2016) 3341–3367, https://doi.org/10.1617/s11527-015-0724-1.

[11] M. Torres-Luque, E. Bastidas-Arteaga, F. Schoefs, M. Sánchez-Silva, J.F. Osma, Non-destructive methods for measuring chloride ingress into concrete: state-of-the-art and future challenges, Constr. Build. Mater. 68 (2014) 68–81, https://doi.org/10.1016/j.conbuildmat.2014.06.009.
[12] S.P. Singh, N. Singh, Reviewing the carbonation resistance of concrete, J. Mater. Eng. Struct. «JMES» 3 (2) (2016) 35–57.
[13] M. Elsalamawy, A.R. Mohamed, E.M. Kamal, The role of relative humidity and cement type on carbonation resistance of concrete, Alex. Eng. J. 58 (2019) 1257–1264, https://doi.org/10.1016/j.aej.2019.10.008.
[14] A. Leemann, P. Nygaard, J. Kaufmann, R. Loser, Relation between carbonation resistance, mix design and exposure of mortar and concrete, Cem. Concr. Compos. 62 (2015) 33–43, https://doi.org/10.1016/j.cemconcomp.2015.04.020.
[15] C. Shi, T.S. He, G. Zhang, X. Wang, Y. Hu, Effects of superplasticizers on carbonation resistance of concrete, Constr. Build. Mater. 108 (2016) 48–55, https://doi.org/10.1016/j.conbuildmat.2016.01.037.
[16] M.A.S. Matos, S.T. Pinho, V.L. Tagarielli, Application of machine learning to predict the multiaxial strain-sensing response of CNT-polymer composites, Carbon N. Y. 146 (2019) 265–275, https://doi.org/10.1016/j.carbon.2019.02.001.
[17] T.V. Nagaraju, S. Mantena, M. Azab, S.S. Alisha, C. El Hachem, M. Adamu, P.S. Rama Murthy, Prediction of high strength ternary blended concrete containing different silica proportions using machine learning approaches, Results Eng. 17 (2023), https://doi.org/10.1016/j.rineng.2023.100973.
[18] B.A. Salami, T. Olayiwola, T.A. Oyehan, I.A. Raji, Data-driven model for ternary-blend concrete compressive strength prediction using machine learning approach, Constr. Build. Mater. 301 (2021), https://doi.org/10.1016/j.conbuildmat.2021.124152.
[19] H. Naseri, H. Jahanbakhsh, P. Hosseini, F. Moghadas Nejad, Designing sustainable concrete mixture by developing a new machine learning technique, J. Clean. Prod. 258 (2020), https://doi.org/10.1016/j.jclepro.2020.120578.
[20] P. Ziolkowski, M. Niedostatkiewicz, Machine learning techniques in concrete mix design, Materials 12 (2019), https://doi.org/10.3390/ma12081256.
[21] R. Cook, T. Han, A. Childers, C. Ryckman, K. Khayat, H. Ma, J. Huang, A. Kumar, Machine learning for high-fidelity prediction of cement hydration kinetics in blended systems, Mater. Des. 208 (2021), https://doi.org/10.1016/j.matdes.2021.109920.
[22] I. Navarrete, I.La Fé-Perdomo, J.A. Ramos-Grez, M. Lopez, Predicting the evolution of static yield stress with time of blended cement paste through a machine learning approach, Constr. Build. Mater. 371 (2023), https://doi.org/10.1016/j.conbuildmat.2023.130632.
[23] F. Aslam, M.Z. Shahab, Supplementary cementitious materials in blended cement concrete: advancements in predicting compressive strength through machine learning, Mater. Today Commun. 38 (2024), https://doi.org/10.1016/j.mtcomm.2023.107725.
[24] G. Ozcan, Y. Kocak, E. Gulbandilar, Estimation of compressive strength of BFS and WTRP blended cement mortars with machine learning models, Comput. Concr. 19 (2017) 275–282, https://doi.org/10.12989/cac.2017.19.3.275.
[25] F. Kang, Y. Wu, J. Ma, J. Li, Structural identification of super high arch dams using Gaussian process regression with improved salp swarm algorithm, Eng. Struct. 286 (2023) 116150, https://doi.org/10.1016/j.engstruct.2023.116150.
[26] J. Zhong, L. Feng, Y.S. Ong, Gene expression programming: a survey [review article, IEEE Comput. Intell. Mag. 12 (2017) 54–72, https://doi.org/10.1109/MCI.2017.2708618.
[27] L. Teodorescu, D. Sherwood, High energy physics event selection with gene expression programming, Comput. Phys. Commun. 178 (2008) 409–419, https://doi.org/10.1016/j.cpc.2007.10.003.
[28] M. Oltean, D. Dumitrescu, Multi expression programming, J. Genet. Program. Evol. Mach. (2002).
[29] A.H. Alavi, A.H. Gandomi, M.G. Sahab, M. Gandomi, Multi expression programming: a new approach to formulation of soil classification, Eng. Comput. 26 (2010) 111–118, https://doi.org/10.1007/s00366-009-0140-7.
[30] S. Sharifi, S. Abrishami, A.H. Gandomi, Consolidation assessment using multi expression programming, Appl. Soft Comput. J. 86 (2020), https://doi.org/10.1016/j.asoc.2019.105842.
[31] A.H. Gandomi, A. Faramarzifar, P.G. Rezaee, A. Asghari, S. Talatahari, New design equations for elastic modulus of concrete using multi expression programming, J. Civ. Eng. Manag. 21 (2015) 761–774, https://doi.org/10.3846/13923730.2014.893910.
[32] M.S. Meddah, M.C. Lmbachiya, R.K. Dhir, Potential use of binary and composite limestone cements in concrete production, Constr. Build. Mater. 58 (2014) 193–205, https://doi.org/10.1016/j.conbuildmat.2013.12.012.
[33] S.-C. Kou, C.-S. Poon, Long-term mechanical and durability properties of recycled aggregate concrete prepared with the incorporation of fly ash, Cem. Concr. Compos. 37 (2013) 12–19, https://doi.org/10.1016/j.cemconcomp.2012.12.011.
[34] M.P. Preez, Sensitivity of strength and durability properties of blended cement concrete to changes in water/binder ratio and binder content, University of the Witwatersrand, Johannesburg Doctoral dissertation, 2019.
[35] H. Quan, H. Kasami, Experimental study on durability improvement of fly ash concrete with durability improving admixture, Sci. World J. 2014 (2014) 1–11, https://doi.org/10.1155/2014/818103.
[36] M. Rathnarajan, S., Vaddey, N.P., Pillai, R.G., Gettu, and Santhanam, R., Modelling carbonation rates in concretes with similar strength and with and without slag., in: Conf. ICACMS, Chennai, India., 2017.
[37] E. Rozière, A. Loukili, F. Cussigh, A performance based approach for durability of concrete exposed to carbonation, Constr. Build. Mater. 23 (2009) 190–199, https://doi.org/10.1016/j.conbuildmat.2008.01.006.
[38] H. Ruixia, A study on carbonation for low calcium fly ash concrete under different temperature and relative humidity, Electron. J. Geotech. Eng. (2010) 1871–1877.
[39] P. Saha, P. Debnath, P. Thomas, Prediction of fresh and hardened properties of self-compacting concrete using support vector regression approach, Neural Comput. Appl. 32 (2020) 7995–8010, https://doi.org/10.1007/s00521-019-04267-w.
[40] M. Şahmaran, İ.Ö. Yaman, M. Tokyay, Transport and mechanical properties of self consolidating concrete with high volume fly ash, Cem. Concr. Compos. 31 (2009) 99–106, https://doi.org/10.1016/j.cemconcomp.2008.12.003.
[41] S. Samad, A. Shah, M.C. Limbachiya, Strength development characteristics of concrete produced with blended cement using ground granulated blast furnace slag (GGBS) under various curing conditions, Sādhanā 42 (2017) 1203–1213, https://doi.org/10.1007/s12046-017-0667-z.
[42] R. San Nicolas, M. Cyr, G. Escadeillas, Performance-based approach to durability of concrete containing flash-calcined metakaolin as cement replacement, Constr. Build. Mater. 55 (2014) 313–322, https://doi.org/10.1016/j.conbuildmat.2014.01.063.
[43] B. Felekoğlu, S. Türkel, B. Baradan, Effect of water/cement ratio on the fresh and hardened properties of self-compacting concrete, Build. Environ. 42 (2007) 1795–1802, https://doi.org/10.1016/j.buildenv.2006.01.012.
[44] F.U.A. Shaikh, S.W.M. Supit, Compressive strength and durability properties of high volume fly ash (HVFA) concretes containing ultrafine fly ash (UFFA), Constr. Build. Mater. 82 (2015) 192–205, https://doi.org/10.1016/j.conbuildmat.2015.02.068.
[45] R. Siddique, Performance characteristics of high-volume Class F fly ash concrete, Cem. Concr. Res. 34 (2004) 487–493, https://doi.org/10.1016/j.cemconres.2003.09.002.
[46] M.G. Silva, M.R.M. Saade, V. Gomes, Influence of service life, strength and cement type on life cycle environmental performance of concrete, Rev. Ibracon Estrut. e Mater. 6 (2013) 844–853, https://doi.org/10.1590/S1983-41952013000600002.
[47] G. Sonebi, M. O'Donughue, Keogh, V. 2008. Effect of the Type of Supplementary Materials and Viscosity Enhancing Admixture on the Durability of Self-Compacting Concrete., in: Proc. 11th Int. Conf. Durab. Build. Mater. Components., Istanbul., 2008.
[48] M. Soutsos, F. Kanavaris, A. Hatzitheodorou, Critical analysis of strength estimates from maturity functions, Case Stud. Constr. Mater. 9 (2018) e00183, https://doi.org/10.1016/j.cscm.2018.e00183.
[49] T. Sugi, H., Tsukagoshi, and Ueda, M., Durability of concrete composites containing fly ash and blast furnace slag for use in for precast concrete products., in: Proc. 3rd Int. Conf. Sustain. Constr. Mater. Technol., Kyoto, Japan, 2013.
[50] S. Sujjavanich, P. Suwanvitaya, D. Chaysuwan, G. Heness, Synergistic effect of metakaolin and fly ash on properties of concrete, Constr. Build. Mater. 155 (2017) 830–837, https://doi.org/10.1016/j.conbuildmat.2017.08.072.
[51] S. Tae, C. Baek, S. Shin, Life cycle CO2 evaluation on reinforced concrete structures with high-strength concrete, Environ. Impact Assess. Rev. 31 (2011) 253–260, https://doi.org/10.1016/j.eiar.2010.07.002.

[52] M. Uysal, M. Sumer, Performance of self-compacting concrete containing different mineral admixtures, Constr. Build. Mater. 25 (2011) 4112–4120, https://doi.org/10.1016/j.conbuildmat.2011.04.032.
[53] E. Vejmelková, M. Pavlíková, Z. Keršner, P. Rovnaníková, M. Ondráček, M. Sedlmajer, R. Černý, High performance concrete containing lower slag amount: a complex view of mechanical and durability properties, Constr. Build. Mater. 23 (2009) 2237–2245, https://doi.org/10.1016/j.conbuildmat.2008.11.018.
[54] S. Teng, T.Y.D. Lim, B. Sabet Divsholi, Durability and mechanical properties of high strength concrete incorporating ultra fine Ground Granulated Blast-furnace Slag, Constr. Build. Mater. 40 (2013) 875–881, https://doi.org/10.1016/j.conbuildmat.2012.11.052.
[55] E. Vejmelková, M. Keppert, S. Grzeszczyk, B. Skaliński, R. Černý, Properties of self-compacting concrete mixtures containing metakaolin and blast furnace slag, Constr. Build. Mater. 25 (2011) 1325–1331, https://doi.org/10.1016/j.conbuildmat.2010.09.012.
[56] S.S. Vivek, G. Dhinakaran, Durability characteristics of binary blend high strength SCC, Constr. Build. Mater. 146 (2017) 1–8, https://doi.org/10.1016/j.conbuildmat.2017.04.063.
[57] A. Vollpracht, M. Soutsos, F. Kanavaris, Strength development of GGBS and fly ash concretes and applicability of fib model code's maturity function – a critical review, Constr. Build. Mater. 162 (2018) 830–846, https://doi.org/10.1016/j.conbuildmat.2017.12.054.
[58] D. Vu, P. Stroeven, V. Bui, Strength and durability aspects of calcined kaolin-blended Portland cement mortar and concrete, Cem. Concr. Compos. 23 (2001) 471–478, https://doi.org/10.1016/S0958-9465(00)00091-3.
[59] H. Yazıcı, The effect of silica fume and high-volume Class C fly ash on mechanical properties, chloride penetration and freeze–thaw resistance of self-compacting concrete, Constr. Build. Mater. 22 (2008) 456–462, https://doi.org/10.1016/j.conbuildmat.2007.01.002.
[60] K.Y. Yeau, E.K. Kim, An experimental study on corrosion resistance of concrete with ground granulate blast-furnace slag, Cem. Concr. Res. 35 (2005) 1391–1399, https://doi.org/10.1016/j.cemconres.2004.11.010.
[61] S.-W. Yoo, G.-S. Ryu, J.F. Choo, Evaluation of the effects of high-volume fly ash on the flexural behavior of reinforced concrete beams, Constr. Build. Mater. 93 (2015) 1132–1144, https://doi.org/10.1016/j.conbuildmat.2015.05.021.
[62] H. Zhao, W. Sun, X. Wu, B. Gao, The properties of the self-compacting concrete with fly ash and ground granulated blast furnace slag mineral admixtures, J. Clean. Prod. 95 (2015) 66–74, https://doi.org/10.1016/j.jclepro.2015.02.050.
[63] R.A. Einsfeld, M.S.L. Velasco, Fracture parameters for high-performance concrete, Cem. Concr. Res. 36 (2006) 576–583, https://doi.org/10.1016/j.cemconres.2005.09.004.
[64] D.K. Panesar, R. Zhang, Performance comparison of cement replacing materials in concrete: Limestone fillers and supplementary cementing materials – a review, Constr. Build. Mater. 251 (2020) 118866, https://doi.org/10.1016/j.conbuildmat.2020.118866.
[65] R.G. Pillai, R. Gettu, M. Santhanam, S. Rengaraju, Y. Dhandapani, S. Rathnarajan, A.S. Basavaraj, Service life and life cycle assessment of reinforced concrete systems with limestone calcined clay cement (LC3), Cem. Concr. Res. 118 (2019) 111–119, https://doi.org/10.1016/j.cemconres.2018.11.019.
[66] S. Kumar, B. Rai, R. Biswas, P. Samui, D. Kim, Prediction of rapid chloride permeability of self-compacting concrete using Multivariate Adaptive Regression Spline and Minimax Probability Machine Regression, J. Build. Eng. 32 (2020) 101490, https://doi.org/10.1016/j.jobe.2020.101490.
[67] P. Van den Heede, M. De Schepper, N. De Belie, Accelerated and natural carbonation of concrete with high volumes of fly ash: chemical, mineralogical and microstructural effects, R. Soc. Open Sci. 6 (2019) 181665, https://doi.org/10.1098/rsos.181665.
[68] D.K. Panesar, K.E. Seto, C.J. Churchill, Impact of the selection of functional unit on the life cycle assessment of green concrete, Int. J. Life Cycle Assess. 22 (2017) 1969–1986, https://doi.org/10.1007/s11367-017-1284-0.
[69] L. Chen, C.-H. Kou, S.-W. Ma, Prediction of slump flow of high-performance concrete via parallel hyper-cubic gene-expression programming, Eng. Appl. Artif. Intell. 34 (2014) 66–74, https://doi.org/10.1016/j.engappai.2014.05.005.
[70] H. Fitriani, A. Ahmed, O. Kolawole, F. Hyndman, Y. Idris, R. Rosidawani, Optimizing compressive strength properties of binary blended cement rice husk concrete for road pavement, Trends Sci. 19 (2022) 3972, https://doi.org/10.48048/tis.2022.3972.
[71] S. Inthata, W. Kowtanapanich, R. Cheerarot, Prediction of chloride permeability of concretes containing ground pozzolans by artificial neural networks, Mater. Struct. 46 (2013) 1707–1721, https://doi.org/10.1617/s11527-012-0009-x.
[72] O. Ahmed Mohamed, M. Ati, W. Al Hawat, Implementation of artificial neural networks for prediction of chloride penetration in concrete, Int. J. Eng. Technol. 7 (2018) 47, https://doi.org/10.14419/ijet.v7i2.28.12880.
[73] P. Van den Heede, M. De Keersmaecker, A. Elia, A. Adriaens, N. De Belie, Service life and global warming potential of chloride exposed concrete with high volumes of fly ash, Cem. Concr. Compos. 80 (2017) 210–223, https://doi.org/10.1016/j.cemconcomp.2017.03.020.
[74] D. Law, I. Patnaikuni, A. Adam, T. Molyneaux, Strength, sorptivity and carbonation of geopolymer concrete. in: Challenges, Oppor. Solut. Struct. Eng. Constr., CRC Press, 2009. ⟨https://doi.org/10.1201/9780203859926.ch91⟩.
[75] O.S. Baghabra Al-Amoudi, W.A. Al-Kutti, S. Ahmad, M. Maslehuddin, Correlation between compressive strength and certain durability indices of plain and blended cement concretes, Cem. Concr. Compos. 31 (2009) 672–676, https://doi.org/10.1016/j.cemconcomp.2009.05.005.
[76] E. Opoku Amankwah, Influence of calcined clay pozzolana on strength characteristics of portland cement concrete, Int. J. Mater. Sci. Appl. 3 (2014) 410, https://doi.org/10.11648/j.ijmsa.20140306.30.
[77] D.E. Angulo-Ramirez, R. Mejía de Gutiérrez, W.G. Valencia-Saavedra, M.H.F. De Medeiros, J. Hoppe-Filho, Carbonation of hybrid concrete with high blast furnace slag content and its impact on structural steel corrosion, Mater. ConstrucciónN. 69 (2019) 182, https://doi.org/10.3989/mc.2019.05418.
[78] V.V. Arora, B. Singh, V. Patel, Durability and corrosion studies in prestressed concrete made with blended cement, J. Asian Concr. Fed. 5 (2019) 15–24, https://doi.org/10.18702/acf.2019.06.30.15.
[79] C.D. Atiş, Accelerated carbonation and testing of concrete made with fly ash, Constr. Build. Mater. 17 (2003) 147–152, https://doi.org/10.1016/S0950-0618(02)00116-2.
[80] BB, Durability properties of concrete containing high volume malaysian fly ash, Int. J. Res. Eng. Technol. 03 (2014) 529–533, https://doi.org/10.15623/ijret.2014.0304093.
[81] M.A. Megat Johari, J.J. Brooks, S. Kabir, P. Rivard, Influence of supplementary cementitious materials on engineering properties of high strength concrete, Constr. Build. Mater. 25 (2011) 2639–2648, https://doi.org/10.1016/j.conbuildmat.2010.12.013.
[82] M.L. Berndt, Properties of sustainable concrete containing fly ash, slag and recycled concrete aggregate, Constr. Build. Mater. 23 (2009) 2606–2613, https://doi.org/10.1016/j.conbuildmat.2009.02.011.
[83] C. Bilim, C.D. Atiş, H. Tanyildizi, O. Karahan, Predicting the compressive strength of ground granulated blast furnace slag concrete using artificial neural network, Adv. Eng. Softw. 40 (2009) 334–340, https://doi.org/10.1016/j.advengsoft.2008.05.005.
[84] W.K. Biswas, Y. Alhorr, K.K. Lawania, P.K. Sarker, E. Elsarrag, Life cycle assessment for environmental product declaration of concrete in the Gulf States, Sustain. Cities Soc. 35 (2017) 36–46, https://doi.org/10.1016/j.scs.2017.07.011.
[85] R. Bucher, P. Diederich, G. Escadeillas, M. Cyr, Service life of metakaolin-based concrete exposed to carbonation, Cem. Concr. Res. 99 (2017) 18–29, https://doi.org/10.1016/j.cemconres.2017.04.013.
[86] K. Celik, C. Meral, A. Petek Gursel, P.K. Mehta, A. Horvath, P.J.M. Monteiro, Mechanical properties, durability, and life-cycle assessment of self-consolidating concrete mixtures made with blended portland cements containing fly ash and limestone powder, Cem. Concr. Compos. 56 (2015) 59–72, https://doi.org/10.1016/j.cemconcomp.2014.11.003.
[87] A. Gholampour, T. Ozbakkaloglu, Performance of sustainable concretes containing very high volume Class-F fly ash and ground granulated blast furnace slag, J. Clean. Prod. 162 (2017) 1407–1417, https://doi.org/10.1016/j.jclepro.2017.06.087.
[88] L. Czarnecki, P. Woyciechowski, G. Adamczewski, Risk of concrete carbonation with mineral industrial by-products, KSCE J. Civ. Eng. 22 (2018) 755–764, https://doi.org/10.1007/s12205-017-1623-5.
[89] B.S. Dhanya, M. Santhanam, R. Gettu, R.G. Pillai, Performance evaluation of concretes having different supplementary cementitious material dosages belonging to different strength ranges, Constr. Build. Mater. 187 (2018) 984–995, https://doi.org/10.1016/j.conbuildmat.2018.07.185.
[90] Y. Dhandapani, T. Sakthivel, M. Santhanam, R. Gettu, R.G. Pillai, Mechanical properties and durability performance of concretes with Limestone Calcined Clay Cement (LC3), Cem. Concr. Res. 107 (2018) 136–151, https://doi.org/10.1016/j.cemconres.2018.02.005.

[91] J.J.O.O. and F.S. By M. Collepardi, S. Collepardi, The Influence of Slag and Fly Ash on the Carbonation of Concretes, in: Proc. 8th CANMET/ACI Int. Conf. Fly Ash, Silica Fume, Slag, Nat. Pozzolans Concr. Held May (Pp. 23-29), 2004.
[92] C.S. Poon, S.C. Kou, L. Lam, Compressive strength, chloride diffusivity and pore structure of high performance metakaolin and silica fume concrete, Constr. Build. Mater. 20 (2006) 858–865, https://doi.org/10.1016/j.conbuildmat.2005.07.001.
[93] B.B.L.K. Crouch, R. Hewitt, High volume fly ash concrete World of Coal Ash (WOCA), pp. 1-14 (2007).
[94] A.M. Diab, A.E.M. Abd Elmoaty, A.A. Aly, Long term study of mechanical properties, durability and environmental impact of limestone cement concrete, Alex. Eng. J. 55 (2016) 1465–1482, https://doi.org/10.1016/j.aej.2016.01.031.
[95] P. Dinakar, K.G. Babu, M. Santhanam, Corrosion behaviour of blended cements in low and medium strength concretes, Cem. Concr. Compos. 29 (2007) 136–145, https://doi.org/10.1016/j.cemconcomp.2006.10.005.
[96] P. Dinakar, K.P. Sethy, U.C. Sahoo, Design of self-compacting concrete with ground granulated blast furnace slag, Mater. Des. 43 (2013) 161–169, https://doi.org/10.1016/j.matdes.2012.06.049.
[97] P. Duan, Z. Shui, W. Chen, C. Shen, Enhancing microstructure and durability of concrete from ground granulated blast furnace slag and metakaolin as cement replacement materials, J. Mater. Res. Technol. 2 (2013) 52–59, https://doi.org/10.1016/j.jmrt.2013.03.010.
[98] A. Durán-Herrera, J.M. Mendoza-Rangel, E.U. De-Los-Santos, F. Vázquez, P. Valdez, D.P. Bentz, Accelerated and natural carbonation of concretes with internal curing and shrinkage/viscosity modifiers, Mater. Struct. 48 (2015) 1207–1214, https://doi.org/10.1617/s11527-013-0226-y.
[99] N.U.K. Eguchi, K. Takewaka, T. Yamaguchi, A study on durability of blast furnace slag cement concrete mixed with metakaolin-based artificial pozzolan in actual marine environment, in: Third Int. Conf. Sustain. Constr. Mater. Technol., 2013.
[100] F. Faleschini, M.A. Zanini, K. Brunelli, C. Pellegrino, Valorization of co-combustion fly ash in concrete production, Mater. Des. 85 (2015) 687–694, https://doi.org/10.1016/j.matdes.2015.07.079.
[101] H. Fanghui, W. Qiang, F. Jingjing, The differences among the roles of ground fly ash in the paste, mortar and concrete, Constr. Build. Mater. 93 (2015) 172–179, https://doi.org/10.1016/j.conbuildmat.2015.05.117.
[102] M.R. Garcez, A.B. Rohden, L.G. Graupner de Godoy, The role of concrete compressive strength on the service life and life cycle of a RC structure: case study, J. Clean. Prod. 172 (2018) 27–38, https://doi.org/10.1016/j.jclepro.2017.10.153.
[103] K.-R. Wu, B. Chen, W. Yao, D. Zhang, Effect of coarse aggregate type on mechanical properties of high-performance concrete, Cem. Concr. Res. 31 (2001) 1421–1425, https://doi.org/10.1016/S0008-8846(01)00588-9.
[104] M. Gesoğlu, E. Güneyisi, E. Özbay, Properties of self-compacting concretes made with binary, ternary, and quaternary cementitious blends of fly ash, blast furnace slag, and silica fume, Constr. Build. Mater. 23 (2009) 1847–1854, https://doi.org/10.1016/j.conbuildmat.2008.09.015.
[105] R. Gettu, R.G. Pillai, M. Santhanam, A.S. Basavaraj, S. Rathnarajan, B.S. Dhanya, Sustainability-based decision support framework for choosing concrete mixture proportions, Mater. Struct. 51 (2018) 165, https://doi.org/10.1617/s11527-018-1291-z.
[106] G.L. Golewski, Green concrete composite incorporating fly ash with high strength and fracture toughness, J. Clean. Prod. 172 (2018) 218–226, https://doi.org/10.1016/j.jclepro.2017.10.065.
[107] E. Güneyisi, M. Gesoğlu, E. Özbay, Strength and drying shrinkage properties of self-compacting concretes incorporating multi-system blended mineral admixtures, Constr. Build. Mater. 24 (2010) 1878–1887, https://doi.org/10.1016/j.conbuildmat.2010.04.015.
[108] T.A. Harrison, M.R. Jones, M.D. Newlands, S. Kandasami, G. Khanna, Experience of using the prTS 12390-12 accelerated carbonation test to assess the relative performance of concrete, Mag. Concr. Res. 64 (2012) 737–747, https://doi.org/10.1680/macr.11.00162.
[109] R.A. Hawileh, J.A. Abdalla, F. Fardmanesh, P. Shahsana, A. Khalili, Performance of reinforced concrete beams cast with different percentages of GGBS replacement to cement, Arch. Civ. Mech. Eng. 17 (2017) 511–519, https://doi.org/10.1016/j.acme.2016.11.006.
[110] E. Holt, E., Kuosa, H., Leivo, M., Al-Neshawy, F., Piironen and Sistonen, J., Accounting for coupled deterioration mechanisms for durable concrete containing mineral by-products., in: Proc. 2nd Int. Conf. Sustain. Constr. Mater. Technol. Ancona, Italy (Vol. 3, Pp. 1631-1643), 2010.
[111] H. Shi, B. Xu, X. Zhou, Influence of mineral admixtures on compressive strength, gas permeability and carbonation of high performance concrete, Constr. Build. Mater. 23 (2009) 1980–1985, https://doi.org/10.1016/j.conbuildmat.2008.08.021.
[112] K. Hussain, P. Choktaweekarn, W. Saengsoy, T. Srichan, S. Tangtermsirikul, Effect of cement types, mineral admixtures, and bottom ash on the curing sensitivity of concrete, Int. J. Miner. Metall. Mater. 20 (2013) 94–105, https://doi.org/10.1007/s12613-013-0699-2.
[113] M. Jalal, A. Pouladkhan, O.F. Harandi, D. Jafari, Retracted: comparative study on effects of Class F fly ash, nano silica and silica fume on properties of high performance self compacting concrete, Constr. Build. Mater. 94 (2015) 90–104, https://doi.org/10.1016/j.conbuildmat.2015.07.001.
[114] B.S. Divsholi, T.Y.D. Lim, S. Teng, Durability properties and microstructure of ground granulated blast furnace slag cement concrete, Int. J. Concr. Struct. Mater. 8 (2014) 157–164, https://doi.org/10.1007/s40069-013-0063-y.
[115] J.F. Dong, Q.Y. Wang, Z.W. Guan, H.K. Chai, High-temperature behaviour of basalt fibre reinforced concrete made with recycled aggregates from earthquake waste, J. Build. Eng. 48 (2022), https://doi.org/10.1016/j.jobe.2021.103895.
[116] L. Jiang, Z. Liu, Y. Ye, Durability of concrete incorporating large volumes of low-quality fly ash, Cem. Concr. Res. 34 (2004) 1467–1469, https://doi.org/10.1016/j.cemconres.2003.12.029.
[117] M.R. Jones, R.K. Dhir, B.J. Magee, Concrete containing ternary blended binders: resistance to chloride ingress and carbonation, Cem. Concr. Res. 27 (1997) 825–831, https://doi.org/10.1016/S0008-8846(97)00075-6.
[118] S.T.K. Kaewmanee, Properties of binder systems containing cement, fly ash and limestone powder, 57, Songklanakarin J. Sci. Technol. (2014) 569, 57.
[119] O. Karahan, Transport properties of high volume fly ash or slag concrete exposed to high temperature, Constr. Build. Mater. 152 (2017) 898–906, https://doi.org/10.1016/j.conbuildmat.2017.07.051.
[120] S. Kumar Karri, G.V.R. Rao, P.M. Raju, Strength and durability studies on GGBS concrete, Int. J. Civ. Eng. 2 (2015) 34–41, https://doi.org/10.14445/23488352/IJCE-V2I10P106.
[121] O.R. Kavitha, V.M. Shanthi, G.P. Arulraj, V.R. Sivakumar, Microstructural studies on eco-friendly and durable Self-compacting concrete blended with metakaolin, Appl. Clay Sci. 124-125 (2016) 143–149, https://doi.org/10.1016/j.clay.2016.02.011.
[122] Y. Khodair, B. Bommareddy, Self-consolidating concrete using recycled concrete aggregate and high volume of fly ash, and slag, Constr. Build. Mater. 153 (2017) 307–316, https://doi.org/10.1016/j.conbuildmat.2017.07.063.
[123] A. Khodabakhshian, J. de Brito, M. Ghalehnovi, E. Asadi Shamsabadi, Mechanical, environmental and economic performance of structural concrete containing silica fume and marble industry waste powder, Constr. Build. Mater. 169 (2018) 237–251, https://doi.org/10.1016/j.conbuildmat.2018.02.192.
[124] S.C. Kou, C.S. Poon, D. Chan, Influence of fly ash as cement replacement on the properties of recycled aggregate concrete, J. Mater. Civ. Eng. 19 (2007) 709–717, https://doi.org/10.1061/(ASCE)0899-1561(2007)19:9(709).
[125] W. Wongkeo, P. Thongsanitgarn, A. Ngamjarurojana, A. Chaipanich, Compressive strength and chloride resistance of self-compacting concrete containing high level fly ash and silica fume, Mater. Des. 64 (2014) 261–269, https://doi.org/10.1016/j.matdes.2014.07.042.
[126] J. Khunthongkeaw, S. Tangtermsirikul, T. Leelawat, A study on carbonation depth prediction for fly ash concrete, Constr. Build. Mater. 20 (2006) 744–753, https://doi.org/10.1016/j.conbuildmat.2005.01.052.
[127] S. Kou, C. Poon, F. Agrela, Comparisons of natural and recycled aggregate concretes prepared with the addition of different mineral admixtures, Cem. Concr. Compos. 33 (2011) 788–795, https://doi.org/10.1016/j.cemconcomp.2011.05.009.
[128] R. Kurda, J.D. Silvestre, J. de Brito, Life cycle assessment of concrete made with high volume of recycled concrete aggregates and fly ash, Resour. Conserv. Recycl. 139 (2018) 407–417, https://doi.org/10.1016/j.resconrec.2018.07.004.
[129] S. Lee, W. Park, H. Lee, Life cycle CO2 assessment method for concrete using CO2 balance and suggestion to decrease LCCO2 of concrete in South-Korean apartment, Energy Build. 58 (2013) 93–102, https://doi.org/10.1016/j.enbuild.2012.11.034.
[130] H.Y. Leung, J. Kim, A. Nadeem, J. Jaganathan, M.P. Anwar, Sorptivity of self-compacting concrete containing fly ash and silica fume, Constr. Build. Mater. 113 (2016) 369–375, https://doi.org/10.1016/j.conbuildmat.2016.03.071.

[131] C. Lima, A. Caggiano, C. Faella, E. Martinelli, M. Pepe, R. Realfonzo, Physical properties and mechanical behaviour of concrete made with recycled aggregates and fly ash, Constr. Build. Mater. 47 (2013) 547–559, https://doi.org/10.1016/j.conbuildmat.2013.04.051.

[132] M. Limbachiya, M.S. Meddah, Y. Ouchagour, Use of recycled concrete aggregate in fly-ash concrete, Constr. Build. Mater. (2011), https://doi.org/10.1016/j.conbuildmat.2011.07.023.

[133] Y.Y.W. Ling, T. Pei, Application of ground granulated blast furnace slag in high-performance concrete in China, in: Int. Work. Sustain. Dev. Concr. Technol. Organ. by China Build. Mater. Acad., 2004: pp. 309–317.

[134] S. Liu, Z. Wang, X. Li, Long-term properties of concrete containing ground granulated blast furnace slag and steel slag, Mag. Concr. Res. 66 (2014) 1095–1103, https://doi.org/10.1680/macr.14.00074.

[135] A.L.I. Löfgren, O. Esping, The influence of carbonation and age on salt frost scaling of concrete with mineral additions Materials, in: Syst. Struct. Civ. Eng., Lyngby, Denmark, 2016: pp. 91–100.

[136] X.-Y. Wang, Simulation for optimal mixture design of low-CO2 high-volume fly ash concrete considering climate change and CO2 uptake, Cem. Concr. Compos. 104 (2019) 103408, https://doi.org/10.1016/j.cemconcomp.2019.103408.

[137] G. Long, Y. Gao, Y. Xie, Designing more sustainable and greener self-compacting concrete, Constr. Build. Mater. 84 (2015) 301–306, https://doi.org/10.1016/j.conbuildmat.2015.02.072.

[138] W.-J. Long, K.H. Khayat, A. Yahia, F. Xing, Rheological approach in proportioning and evaluating prestressed self-consolidating concrete, Cem. Concr. Compos. 82 (2017) 105–116, https://doi.org/10.1016/j.cemconcomp.2017.05.008.

[139] A. Lübeck, A.L.G. Gastaldini, D.S. Barin, H.C. Siqueira, Compressive strength and electrical properties of concrete with white Portland cement and blast-furnace slag, Cem. Concr. Compos. 34 (2012) 392–399, https://doi.org/10.1016/j.cemconcomp.2011.11.017.

[140] S. Marinković, J. Dragaš, I. Ignjatović, N. Tošić, Environmental assessment of green concretes for structural use, J. Clean. Prod. 154 (2017) 633–649, https://doi.org/10.1016/j.jclepro.2017.04.015.

[141] P.F. Marques, C. Chastre, Â. Nunes, Carbonation service life modelling of RC structures for concrete with Portland and blended cements, Cem. Concr. Compos. 37 (2013) 171–184, https://doi.org/10.1016/j.cemconcomp.2012.10.007.

[142] P.R. de Matos, R.D. Sakata, L.R. Prudêncio, Eco-efficient low binder high-performance self-compacting concretes, Constr. Build. Mater. 225 (2019) 941–955, https://doi.org/10.1016/j.conbuildmat.2019.07.254.

[143] M. Mccarthy, R. Dhir, Development of high volume fly ash cements for use in concrete construction, Fuel 84 (2005) 1423–1432, https://doi.org/10.1016/j.fuel.2004.08.029.

[144] C. McNally, E. Sheils, Probability-based assessment of the durability characteristics of concretes manufactured using CEM II and GGBS binders, Constr. Build. Mater. 30 (2012) 22–29, https://doi.org/10.1016/j.conbuildmat.2011.11.029.

[145] R.S.A. Mittal, M.B. Kaisare, Experimental Study on use of fly ash in concrete, 2005.

[146] E.G. Moffatt, M.D.A. Thomas, A. Fahim, Performance of high-volume fly ash concrete in marine environment, Cem. Concr. Res. 102 (2017) 127–135, https://doi.org/10.1016/j.cemconres.2017.09.008.

[147] Y. Zhang, C. Song, J. Zhang, H. Bo, L.L. Ji, Exercise training induced anti-inflammatory IL-6 in aged skeletal muscle, Med. Sci. Sport. Exerc. 50 (2018) 198, https://doi.org/10.1249/01.mss.0000535737.45954.59.

[148] J. Mohammadi, W. South, Life cycle assessment (LCA) of benchmark concrete products in Australia, Int. J. Life Cycle Assess. 22 (2017) 1588–1608, https://doi.org/10.1007/s11367-017-1266-2.

[149] Z. Murad, Y. Imam, R. Abu Hajar, H. Habeh, D. Hammad, A. Shawash, Predictive compressive strength models for green concrete, Int. J. Struct. Integr. (2019).

[150] I. Navarro, V. Yepes, J. Martí, Life cycle cost assessment of preventive strategies applied to prestressed concrete bridges exposed to chlorides, Sustainability 10 (2018) 845, https://doi.org/10.3390/su10030845.

[151] M.C.S. Nepomuceno, L.A. Pereira-de-Oliveira, S.M.R. Lopes, Methodology for the mix design of self-compacting concrete using different mineral additions in binary blends of powders, Constr. Build. Mater. 64 (2014) 82–94, https://doi.org/10.1016/j.conbuildmat.2014.04.021.

[152] T. Nochaiya, W. Wongkeo, A. Chaipanich, Utilization of fly ash with silica fume and properties of Portland cement–fly ash–silica fume concrete, Fuel 89 (2010) 768–774, https://doi.org/10.1016/j.fuel.2009.10.003.

[153] A. Oner, S. Akyuz, An experimental study on optimum usage of GGBS for the compressive strength of concrete, Cem. Concr. Compos. 29 (2007) 505–514, https://doi.org/10.1016/j.cemconcomp.2007.01.001.

[154] A. Oner, S. Akyuz, R. Yildiz, An experimental study on strength development of concrete containing fly ash and optimum usage of fly ash in concrete, Cem. Concr. Res. 35 (2005) 1165–1171, https://doi.org/10.1016/j.cemconres.2004.09.031.

[155] J. Park, S. Tae, T. Kim, Life cycle CO2 assessment of concrete by compressive strength on construction site in Korea, Renew. Sustain. Energy Rev. 16 (2012) 2940–2946, https://doi.org/10.1016/j.rser.2012.02.014.

[156] M.E. Parron-Rubio, F. Perez-Garcia, A. Gonzalez-Herrera, M.J. Oliveira, M.D. Rubio-Cintas, Slag substitution as a cementing material in concrete: mechanical, physical and environmental properties, Materials 12 (2019) 2845, https://doi.org/10.3390/ma12182845.

[157] Y.O. Patil, P.N.P. P.N.Patil, D.A.K. Dwivedi, GGBS as partial replacement of OPC in cement concrete – an experimental study, Int. J. Sci. Res. 2 (2012) 189–191, https://doi.org/10.15373/22778179/NOV2013/60.

[158] J.F. Dong, Y. Xu, Z.W. Guan, Q.Y. Wang, Freeze-thaw behaviour of basalt fibre reinforced recycled aggregate concrete filled CFRP tube specimens, Eng. Struct. 273 (2022), https://doi.org/10.1016/j.engstruct.2022.115088.

[159] H. Alabduljabbar, M. Khan, H.H. Awan, S.M. Eldin, R. Alyousef, A.M. Mohamed, Predicting ultra-high-performance concrete compressive strength using gene expression programming method, Case Stud. Constr. Mater. 18 (2023), https://doi.org/10.1016/j.cscm.2023.e02074.

[160] D. Chen, F. Kang, J. Li, S. Zhu, X. Liang, Enhancement of underwater dam crack images using multi-feature fusion, Autom. Constr. 167 (2024), https://doi.org/10.1016/j.autcon.2024.105727.

[161] S. Nazar, J. Yang, M.N. Amin, K. Khan, M.F. Javed, F. Althoey, Formulation of estimation models for the compressive strength of concrete mixed with nanosilica and carbon nanotubes, Dev. Built Environ. 13 (2023) 100113, https://doi.org/10.1016/j.dibe.2022.100113.

[162] R. Alyousef, R.U.D. Nassar, M. Khan, K. Arif, M. Fawad, A.M. Hassan, N.A. Ghamry, Forecasting the strength characteristics of concrete incorporating waste foundry sand using advance machine algorithms including deep learning, Case Stud. Constr. Mater. 19 (2023), https://doi.org/10.1016/j.cscm.2023.e02459.

[163] M. Alyami, R.U.D. Nassar, M. Khan, A.W. Hammad, H. Alabduljabbar, R. Nawaz, M. Fawad, Y. Gamil, Estimating compressive strength of concrete containing rice husk ash using interpretable machine learning-based models, Case Stud. Constr. Mater. 20 (2024), https://doi.org/10.1016/j.cscm.2024.e02901.

[164] H. Chauhan, Y. Jang, S. Pradhan, H. Moon, Personalized optimal room temperature and illuminance for maximizing occupant's mental task performance using physiological data, J. Build. Eng. 78 (2023), https://doi.org/10.1016/j.jobe.2023.107757.

[165] Y. Jang, I. Jeong, M. Younesi Heravi, S. Sarkar, H. Shin, Y. Ahn, Multi-camera-based human activity recognition for human–robot collaboration in construction, Sensors 23 (2023), https://doi.org/10.3390/s23156997.

[166] M.N. Amin, M.F. Javed, K. Khan, F.I. Shalabi, M.G. Qadir, Modeling compressive strength of eco-friendly volcanic ash mortar using artificial neural networking, Symmetry 13 (2021), https://doi.org/10.3390/sym13112009.

[167] R. Alyousef, M.F. Rehman, M. Khan, M. Fawad, A.U. Khan, A.M. Hassan, N.A. Ghamry, Machine learning-driven predictive models for compressive strength of steel fiber reinforced concrete subjected to high temperatures, Case Stud. Constr. Mater. 19 (2023), https://doi.org/10.1016/j.cscm.2023.e02418.

[168] M. Khan, M. Ali, T. Najeh, Y. Gamil, Computational prediction of workability and mechanical properties of bentonite plastic concrete using multi-expression programming, Sci. Rep. 14 (2024), https://doi.org/10.1038/s41598-024-56088-0.

[169] M. Khan, A. Khan, A.U. Khan, M. Shakeel, K. Khan, H. Alabduljabbar, T. Najeh, Y. Gamil, Intelligent prediction modeling for flexural capacity of FRP-strengthened reinforced concrete beams using machine learning algorithms, Heliyon 10 (2024), https://doi.org/10.1016/j.heliyon.2023.e23375.

[170] C. Ferreira, Automatically Defined Functions in Gene Expression Programming, 2006.

[171] C. Ferreira, Gene Expression Programming: Mathematical Modeling by an Artificial Intelligence, 2006.

[172] M. Khan, R.U.D. Nassar, W. Anwar, M. Rasheed, T. Najeh, Y. Gamil, F. Farooq, Forecasting the strength of graphene nanoparticles-reinforced cementitious composites using ensemble learning algorithms, Results Eng. 21 (2024), https://doi.org/10.1016/j.rineng.2024.101837.
[173] M. Khan, M. Shakeel, K. Khan, S. Akbar, A. Khan, A review on fiber-reinforced foam concrete, Eng. Proc. 22 (2022), https://doi.org/10.3390/engproc2022022013.
[174] A. Khan, M. Khan, M. Ali, M. Khan, A.U. Khan, M. Shakeel, M. Fawad, T. Najeh, Y. Gamil, Predictive modeling for depth of wear of concrete modified with fly ash: a comparative analysis of genetic programming-based algorithms, Case Stud. Constr. Mater. 20 (2024), https://doi.org/10.1016/j.cscm.2023.e02744.
[175] S. Lundberg, Commentary, Ann. Emerg. Med. 70 (2017) 30–31, https://doi.org/10.1016/j.annemergmed.2017.05.019.
[176] M. Khan, R.U.D. Nassar, A.U. Khan, M. Houda, C. El Hachem, M. Rasheed, W. Anwar, Optimizing durability assessment: machine learning models for depth of wear of environmentally-friendly concrete, Results Eng. 20 (2023), https://doi.org/10.1016/j.rineng.2023.101625.
[177] A. Aldrees, M. Khan, A.T.B. Taha, M. Ali, Evaluation of water quality indexes with novel machine learning and shapley additive explanation (SHAP) approaches, J. Water Process Eng. 58 (2024), https://doi.org/10.1016/j.jwpe.2024.104789.
[178] M. Scott, Lundberg and Sun-In Lee, A Unified Approach to Interpreting Model Predictions. NeurIPS Proceedings, (2017).
[179] F. Lollini, E. Redaelli, Carbonation of blended cement concretes after 12 years of natural exposure, Constr. Build. Mater. 276 (2021), https://doi.org/10.1016/j.conbuildmat.2020.122122.
[180] D. Jozwiak-Niedzwiedzka, Influence of blended cements on the concrete resistance to carbonation, BMC 2010, Brittle Matrix Compos 10 (2012) 125–134, https://doi.org/10.1533/9780857099891.125.
[181] H. Huang, C. Qian, F. Zhao, J. Qu, J. Guo, M. Danzinger, Improvement on microstructure of concrete by polycarboxylate superplasticizer (PCE) and its influence on durability of concrete, Constr. Build. Mater. 110 (2016) 293–299, https://doi.org/10.1016/j.conbuildmat.2016.02.041.
[182] J. Liu, X. Wang, Q. Qiu, G. Ou, F. Xing, Understanding the effect of curing age on the chloride resistance of fly ash blended concrete by rapid chloride migration test, Mater. Chem. Phys. 196 (2017) 315–323, https://doi.org/10.1016/j.matchemphys.2017.05.011.
[183] H. Yildirim, T. Ilica, O. Sengul, Effect of cement type on the resistance of concrete against chloride penetration, Constr. Build. Mater. 25 (2011) 1282–1288, https://doi.org/10.1016/j.conbuildmat.2010.09.023.
[184] L.G. Li, J.Y. Zheng, P.L. Ng, J. Zhu, A.K.H. Kwan, Cementing efficiencies and synergistic roles of silica fume and nano-silica in sulphate and chloride resistance of concrete, Constr. Build. Mater. 223 (2019) 965–975, https://doi.org/10.1016/j.conbuildmat.2019.07.241.
[185] K.K. Sideris, A.E. Savva, J. Papayianni, Sulfate resistance and carbonation of plain and blended cements, Cem. Concr. Compos. 28 (2006) 47–56, https://doi.org/10.1016/j.cemconcomp.2005.09.001.
[186] S.J. Kwon, X.Y. Wang, CO2 uptake model of limestone-powder-blended concrete due to carbonation, J. Build. Eng. 38 (2021), https://doi.org/10.1016/j.jobe.2021.102176.
[187] J.H. Friedman, Greedy function approximation: a gradient boosting machine, Ann. Stat. 29 (2001) 1189–1232, https://doi.org/10.1214/aos/1013203451.
[188] A. Kashem, R. Karim, S.C. Malo, P. Das, S.D. Datta, M. Alharthai, Hybrid data-driven approaches to predicting the compressive strength of ultra-high-performance concrete using SHAP and PDP analyses, Case Stud. Constr. Mater. 20 (2024), https://doi.org/10.1016/j.cscm.2024.e02991.
[189] J.B.& E.P. Alex Goldstein, Adam Kapelner, Peeking Inside the Black Box: Visualizing Statistical Learning With Plots of Individual Conditional Expectation, (2015).
[190] M. Rajczakowska, M. Szeląg, K. Habermehl-Cwirzen, H. Hedlund, A. Cwirzen, Interpretable machine learning for prediction of post-fire self-healing of concrete, Materials 16 (2023), https://doi.org/10.3390/ma16031273.
[191] E. Güneyisi, T. Özturan, M. Gesoğlu, Effect of initial curing on chloride ingress and corrosion resistance characteristics of concretes made with plain and blended cements, Build. Environ. 42 (2007) 2676–2685, https://doi.org/10.1016/j.buildenv.2006.07.008.
[192] K. Kopecskó, G.L. Balázs, Concrete with improved chloride binding and chloride resistivity by blended cements, Adv. Mater. Sci. Eng. 2017 (2017), https://doi.org/10.1155/2017/7940247.
[193] N. Flores Medina, G. Barluenga, F. Hernández-Olivares, Combined effect of Polypropylene fibers and Silica Fume to improve the durability of concrete with natural Pozzolans blended cement, Constr. Build. Mater. 96 (2015) 556–566, https://doi.org/10.1016/j.conbuildmat.2015.08.050.
[194] H. Kim, R. Sharma, J. Pei, J.G. Jang, Effect of carbonation curing on physicochemical properties of mineral admixture blended belite-rich cement, J. Build. Eng. 56 (2022), https://doi.org/10.1016/j.jobe.2022.104771.